Gondwana Research 125 (2024) 317–342

Contents lists available at ScienceDirect

Gondwana Research

journal homepage: www.elsevier.com/locate/gr

Carbonatite and ultrabasic magmatism at Toro Ankole and Virunga, western branch of the East African Rift system

Francesca Innocenzi [a,b,*], Sara Ronca [a], Stephen Foley [c], Samuele Agostini [b], Michele Lustrino [a,d]

[a] Dipartimento di Scienze della Terra, Sapienza Università di Roma, P.le A. Moro, 5, 00185 Roma, Italy
[b] Istituto di Geoscienze e Georisorse – CNR, Via Moruzzi, 1, 56124 Roma, Italy
[c] School of Natural Sciences, Macquarie University, North Ryde, New South Wales 2109, Australia
[d] Istituto di Geologia Ambientale e Geoingegneria – CNR, c/o Dipartimento di Scienze della Terra, Sapienza Università di Roma, P.le A. Moro, 5, 00185 Roma, Italy

ARTICLE INFO

Article history:
Received 21 January 2023
Revised 1 August 2023
Accepted 5 September 2023
Available online 9 September 2023
Handling Editor: L. Tang

Keywords:
East African Rift
Alkaline magmatism
Kalsilite-bearing rocks
Carbonatites

ABSTRACT

The western branch of the East African Rift hosts four main Neogene-Quaternary volcanic provinces, characterized by products with wide chemical and mineralogical variability. This study focuses on the two northernmost volcanic provinces, Toro Ankole where ~0.2 Ma-old carbonatites, melilitites and kamafugites, erupted together with foidites, and Virunga where ~13–9 Ma-old strongly and mildly alkaline rocks, from nephelinite up to trachytes crop out. Petrographic and whole/rock geochemical characteristics (low SiO_2, high CaO and K_2O, coupled with LILE enrichment) of 49 samples from Toro Ankole and 5 samples from Virunga (tephrites, trachybasalts and trachyandesites) point out enriched and heterogeneous sub-lithospheric mantle sources. The nature of the ultramafic nodules occasionally associated to the investigated samples highlights the presence of metasomatic veins variably enriched in clinopyroxene, phlogopite, carbonate, apatite, Ti-magnetite and titanite. $^{143}Nd/^{144}Nd$ ratios of Toro Ankole rocks are below ChUR (0.51249–0.51260), and all but two carbonatite lavas have $^{87}Sr/^{86}Sr$ > BSE (0.7046–0.7056). Virunga lavas display less radiogenic $^{143}Nd/^{144}Nd$ (0.51235–0.51249) and more radiogenic $^{87}Sr/^{86}Sr$ ratios (0.7058–0.7071). Lead isotopes are all above the NHRL ($^{206}Pb/^{204}Pb$ mostly in the range 19.12–19.63). $\delta^{11}B$ values cover the whole OIB range (−8.3 to −3.3 ‰), but with the exception of some Toro Ankole samples with notably heavier compositions (−1.9 to 6.6), here linked to the carbonate enrichment. The differences in the isotopic features observed between Toro Ankole and Virunga products may reflect a north to south change of the lithospheric mantle source in terms of composition, mineralogy and depth of melting. Toro Ankole phlogopite-bearing mantle is more intensely metasomatized by a ^{87}Sr- and ^{11}B-rich component (as altered oceanic crust or subducted carbonates) compare to that one beneath Virunga, in which the metasomes might contain amphibole rather than phlogopite. Low degree of partial melting of the metasomatized mantle produces magmas of carbonatitic and ultrabasic/ultrapotassic compositions of the western rift branch.

1. Introduction

Exotic and rare igneous lithologies such as carbonatites, melilitites, leucitites and kamafugites have always attracted the attention of Earth scientists (e.g., Holmes and Harwood, 1932; Lloyd et al., 1985; Edgar and Vukadinovic, 1992; Mitchell, 2020; Lustrino et al., 2019a, 2020, 2022a; Yaxley et al., 2022). Exploration industry is interested in these compositions too, because some of them host exploitable concentrations of ore minerals (e.g., Krmíček and Chalapathi Rao, 2021). The study of these exotic igneous rocks is helpful in deciphering the thermal state and chemical composition of the mantle, shedding light on its heterogeneities. In addition, understanding carbonatitic magmatism is important for calibrating chemical exchanges between reservoirs in the deep carbon cycle. Despite their importance the IUGS guidelines for classification and nomenclature fail to properly identify and definitively classify exotic compositions such as carbonatites, lamprophyres, lamproites, kimberlites and kamafugites, and various, albeit not yet fully accepted classification schemes are available (e.g., Scott Smith et al., 2018; Mitchell, 2020; Mitchell and Gittins, 2022; Oliveira et al., 2022; Tappe et al., 2022).

* Corresponding author at: Dipartimento di Scienze della Terra, Sapienza Università di Roma, P.le A. Moro, 5, 00185 Roma, Italy.
E-mail address: francesca.innocenzi@uniroma1.it (F. Innocenzi).

https://doi.org/10.1016/j.gr.2023.09.005
1342-937X/

The western branch of the East African Rift (hereafter WEAR) offers a rare chance to study carbonatites, melilitites, kamafugites, nephelinites and leucitites together, as they occur in a relatively restricted area (e.g., Holmes and Harwood, 1932; Sahama, 1974). Despite the petrographic and geochemical relevance of these rocks, the number of articles dealing with the igneous activity of the WEAR is relatively small. This contribution aims to review and improve on this knowledge, presenting new data for 34 samples (the most representative and freshest from the set of 49 rocks) along with a compilation of literature analyses (855 whole/rock analyses). Among the most unusual rock types, the archetypal kamafugites occur in this area and for this reason we concentrate on this rock association.

1.1. Kamafugites

Kamafugite is a collective term originally introduced by Sahama (1974) to group kalsilite-bearing volcanic rocks characterized by alkaline, often perpotassic (i.e., K/Al > 1), silica-undersaturated compositions. Kamafugite is an acronym derived from the three first kalsilite-bearing volcanic rock types found in Uganda, namely KAtungite (kalsilite-olivine-melilitite), MAFurite (olivine-melilite-kalsilitite) and UGandite (olivine-kalsilite-leucitite; Holmes, 1950; Sahama, 1974). Nowadays, the IUGS prefers to group kamafugite under the "kalsilite-bearing volcanic rocks" heading, excluding ugandites from this rock group and including two other rock types such as (kalsilite-phlogopite-olivine-leucite melilitite) and coppaelite (kalsilite-phlogopite melilitite; see a review in Lustrino et al., 2020). The IUGS (Woolley et al., 1996; Le Maitre, 2002) excluded ugandites from the "kalsilite-bearing volcanic rocks" because of the assumed absence of this mineral in these rocks. Interestingly, kalsilite was instead identified and analysed in the type locality of ugandite (Kazimiro crater, Bunyaruguru, Uganda; Tappe et al., 2003) just one year after the release of the second edition of the IUGS book.

Oliveira et al. (2022), to clarify the controversial IUGS classification for kalsilite-bearing rocks suggested an improvement, based on petrographic and textural features, highlighting only four end members; katungite, ugandite, mafurite and kalsilite nephelinite. They also suggested for kamafugites a classification based on chemical grounds only.

Kamafugites (Group II of ultrapotassic rocks; Foley et al. 1987) are chemically characterized by low SiO_2 (<46 wt%) and high CaO contents coupled with low Al_2O_3 and Na_2O, and Mg# [Mg# = M g/(Mg + Fe)] > 60. Other than fundamental kalsilite, the mineral assemblage of kamafugites commonly includes olivine, clinopyroxene, phlogopite, leucite, melilite, perovskite and carbonate in the groundmass, not all necessarily present in the same rock. A peculiar characteristic is the lack of any feldspar, owing to the low Al_2O_3 and SiO_2 contents (Foley et al., 1987; Le Maitre, 2002; Lustrino et al., 2020; Oliveira et al., 2022).

Igneous rocks with primary kalsilite have been recorded in three localities worldwide only: (1) Central Italy (Intra Apennine Province; San Venanzo and Cupaello; Lustrino et al., 2020, 2022a); (2) SE Brazil (Alto Paranaiba and Goiás Alkaline Province; Brod et al., 2000; Melluso et al., 2008; Velasquez Ruiz et al., 2022); and (3) WEAR (Toro Ankole and Virunga; Holmes, 1942, 1950, 1952; Sahama, 1957; Tappe et al., 2003; Rosenthal et al., 2009; Muravyeva et al., 2014). Despite their rarity, kamafugites have been found in different geodynamic settings. For example, the Italian localities occur in a subduction-related setting (Lustrino et al., 2020), whereas the Brazilian and Ugandan kamafugites were emplaced in intraplate and active continental rift settings (Tappe et al., 2003; Melluso et al., 2008).

2. Geological background

The East African Rift System (EAR; Fig. 1) is a complex, roughly N-S-oriented, active continental rift zone, mainly developed along previous Proterozoic mobile belt and separated into eastern and western branches by the Tanzanian Craton (Roberts et al., 2012; Michon et al., 2022). The crust of the Tanzanian Craton mainly consists of Meso- to Neo-Archean (~2.6–2.9 Ga) metavolcanic, metasedimentary, gneissic and migmatitic basement rocks (Thomas et al., 2016). It is bound to the west by the Karagwe-Ankole and Ubendian Belts, where the WEAR developed, and to the east by the Mozambique Belt, parallel to the eastern Branch of the EAR system. These two branches join south of the Tanzanian Craton, and then are split again into the Okavango and Malawi Rifts (Michon et al., 2022).

The Main Ethiopian Rift in the north and the eastern branch of EAR can be traced for ~3000 km in length, from the Afar area to Lake Malawi (Chorowicz, 2005; Rooney, 2020a). The WEAR has a total length of ~2100 km, stretching from Lake Albert in the north, to Lake Malawi in the south, through a series of rift segments known as the Albertine, Tanganyika, Rukwa and Malawi rifts, (Ebinger, 1989; Chorowicz, 2005; Michon et al., 2022; Fig. 1b). The onset of the extensional regime and rifting phases occurred diachronously in the eastern (~40–35 Ma) and western branches (~12 Ma; Ebinger, 1989; Pouclet et al., 2016), although recent studies have identified an earlier rifting phase for the western branch, dated back to the Oligocene (~25 Ma in the Rukwa rift, Roberts et al., 2012; Jess et al., 2020; Michon et al., 2022; Lawrence et al., 2022). The two branches differ greatly (Rooney, 2020a, 2020b) in three main characteristics:

(1) The beginning of igneous activity. In the eastern branch (Turkana depression in northern Kenya) the first volcanism is dated ~40–45 Ma vs. ~20 Ma in the western branch in the Lake Kivu area (Kampunzu and Mohr, 1991; Furman et al., 2006; Pouclet et al., 2016; Rooney, 2017; Michon et al., 2022);
(2) The estimated amount of emplaced magma. The eastern branch is characterized by much more voluminous (~900.000 km^3) igneous activity compared to the western branch (100.000 km^3; Kampunzu and Mohr, 1991; Roberts et al., 2012; Minissale, 2017);
(3) The composition of the igneous products. In the WEAR carbonatites and potassic/ultrapotassic ultrabasic up to alkaline products are relatively common, plus limited amounts of more differentiated members, such as trachytes. On the other hand, EAR is characterized by mostly sodic alkaline rocks with diffuse evolved lithologies (trachytes and peralkaline rhyolites in many caldera-forming eruptions in the Ethiopian Rift; Kampunzu and Mohr, 1991; Pouclet et al., 2016; Rapprich et al., 2016), plus rarer ultra-alkaline and carbonatite types (e.g., S Kenya Rift with the active volcano Oldoinyo Lengai; Kampunzu and Mohr, 1991; Pouclet et al., 2016).

2.1. Igneous activity

The WEAR is characterized by the presence of abundant but scattered igneous products that can be grouped into four main volcanic provinces (Fig. 1a). From north to south, these are: Toro Ankole (western Uganda), Virunga (straddling the political borders of Uganda, Rwanda and the Democratic Republic of Congo), South Kivu (including the two volcanic fields of Bukavu and Mwenga-Kamituga in Rwanda and Democratic Republic of Congo) and Rungwe (SW Tanzania; Auchapt et al., 1987; Marcelot et al.,

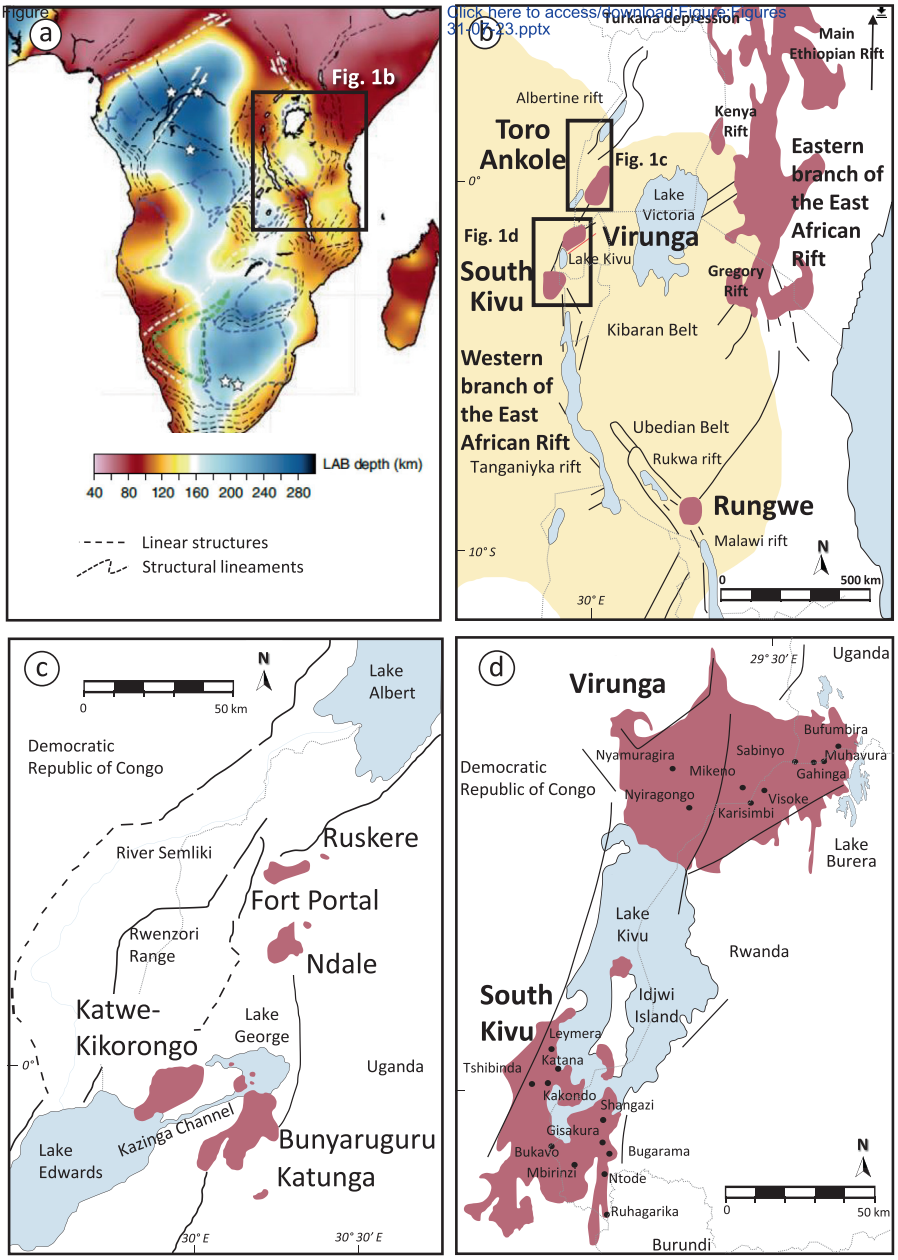

Fig. 1. Map of western rift volcanic fields in the context of African geology. (a) The thickness of the lithosphere, highlighting the presence of different cratons. From Afonso et al. (2022). (b) Sketch map of the four volcanic provinces of the WEAR (Toro Ankole, Virunga, South Kivu and Rungwe). The eastern branch is also outlined. Black lines: main faults; light yellow area = Tanzanian craton. Modified after Rosenthal et al., 2009, Roberts et al., 2012. (c) Toro Ankole volcanic field, consisting of Fort Portal, Ndale, Katwe-Kikorongo and Bunyarguru, plus Katunga. Black lines: main faults. Modified after Rosenthal et al., 2009. (d) Virunga and the South Kivu volcanic provinces and their main eruptive centres. Modified after Furman and Graham, 1999 and Muravyeva et al., 2021. (For interpretation of the references to colour in this figure legend, the reader is referred to the web version of this article.)

1989; Furman, 1995; Rosenthal et al., 2009, Pouclet et al., 2016: Michon et al., 2022; Fig. 1b). Rungwe occurs at the southern convergence of the two branches (Fontijn et al., 2012) but is usually related to the WEAR (e.g., Furman, 1995; Furman and Graham, 1999). The volcanic activity in the WEAR started ~21 Ma (K-Ar age; Pouclet et al., 2016) during a pre-rift stage with emplacement of nephelinite lava flow in the North Idjwi (Lake Kivu Island). In the mid Miocene, sodic alkali basaltic products were erupted in west Virunga (~13–9 Ma; K-Ar; Pouclet et al., 2016) during the formation of N-S striking rift basins. Later, magmatism and rifting reached the South Kivu province at ~11–8 Ma (K-Ar; Ebinger et al., 1989; Pouclet et al., 2016). Eventually, volcanism took place further north in the Toro Ankole area (~188 ka, $^{40}Ar/^{39}Ar$; Rosenthal et al., 2009; Pitcavage et al., 2021). The beginning of igneous activity in the Rungwe volcanic province is still debated (Rooney, 2020b), ranging from ~9 Ma (Ebinger, 1989; Furman, 1995) to ~19 Ma ($^{40}Ar/^{39}Ar$; Mesko, 2020) or even ~26 Ma (U-Pb and $^{40}Ar/^{39}Ar$; Roberts et al., 2012; Michon et al., 2022).

WEAR magmatism is characterized by a wide compositional range (from nearly pure carbonatites, with SiO_2 ~ 5 wt% to trachytes, with SiO_2 ~ 62 wt%; Fig. 2a). Ultrabasic compositions (SiO_2 < 45 wt%) are particularly abundant in the Toro Ankole and Rungwe fields (mostly ~35–45 wt% SiO_2). The WEAR rocks are characterized by a large range of K_2O/Na_2O ratios (Fig. 2b), with compositions ranging from sodic (K_2O/Na_2O < 0.6 in Rungwe and Kivu), through mildly potassic (K_2O/Na_2O mostly from 0.5 to 2

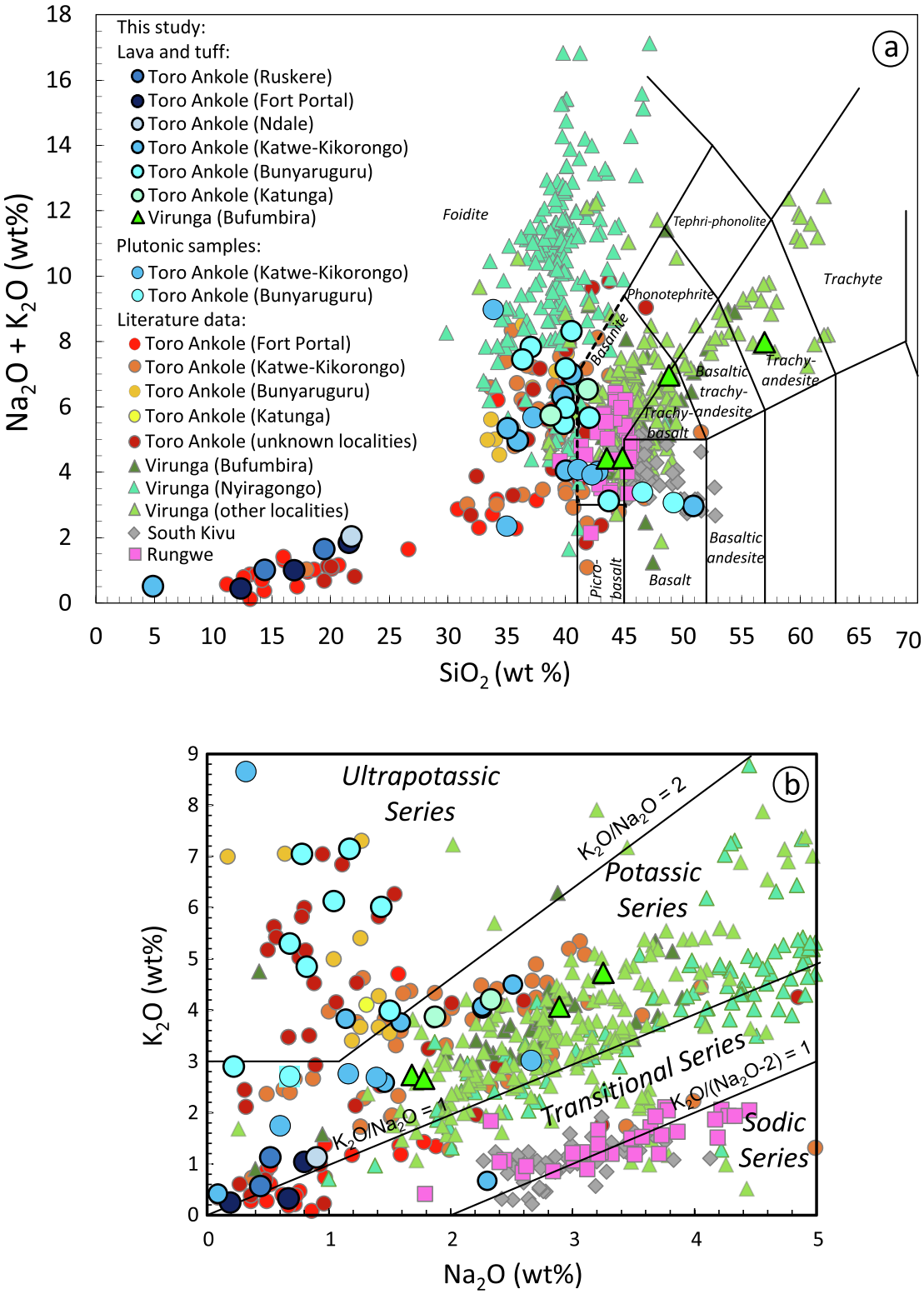

Fig. 2. (a) TAS diagram (Total alkali vs silica; Le Maitre, 2002) showing Toro Ankole (Fort Portal, Rusekere, Katwe-Kikorongo, Ndale, Bunyaruguru, Katunga) and Virunga (Bufumbira) rocks. Symbols with thick black rims are lavas and tuffs; symbols with thin black rims are plutonic samples (melanocratic foidolites and ultramafic nodules). Published data for Toro Ankole (Ödman, 1930; Smith, 1931; Holmes and Harwood, 1932; Holmes, 1937, 1942, 1950, 1952, 1956; Combe and Holmes, 1945; Higazy, 1954; Bell and Powell, 1969; Nixon and Hornung, 1973; Mitchell and Bell, 1976; Barker and Nixon, 1989; Stoppa et al., 2000; Tappe et al., 2003; Eby et al., 2009; Rosenthal et al., 2009, Muravyeva et al., 2014; Murav'eva and Senin, 2009; Foley et al., 2011; Stoppa and Schiazza, 2013; Pitcavage et al., 2021), Virunga (Finckh, 1912; Lacroix 1923; Holmes, 1936; Holmes and Harwood, 1936, 1937; Sahama, 1953, 1962a, 1978; Higazy, 1954; Denaeyer, 1956, 1960, 1965, 1972; Denaeyer et al., 1957; Sahama and Meyer, 1958; Bell and Powell, 1969; Bell and Doyle, 1971; Tilley and Thompson, 1972; Pouclet, 1973; Thompson, 1975; Mitchell and Bell, 1976; Nakamura and Aoki, 1980; Pouclet et al., 1983, 2016; Vollmer and Norry, 1983; Aoki et al., 1985; Hertogen et al., 1985; Marcelot et al., 1985, 1989; Mulder et al., 1986; Marcelot and Rançon, 1988; Williams and Gill, 1992; Rogers et al., 1992, 1998; Demant et al., 1994; Pickett and Murrell, 1997; Capaccioni et al., 2002; Santo et al., 2003; Platz et al., 2004; Chakrabarti et al., 2009; Foley et al., 2012; Andersen et al., 2012; Muravyeva et al., 2014, 2021; Condomines et al., 2015; Barette et al., 2017; Minissale et al., 2017, 2019, 2022; Pitcavage et al., 2021), South Kivu (Auchapt et al., 1987; Marcelot et al., 1989; Furman and Graham, 1999; Pouclet et al., 2016) and Rungwe (Marcelot et al., 1989; Furman, 1995) are also plotted for comparison. (b) K_2O vs Na_2O diagram with ultrapotassic, potassic, transitional and sodic fields. Symbols as in Fig. 2a.

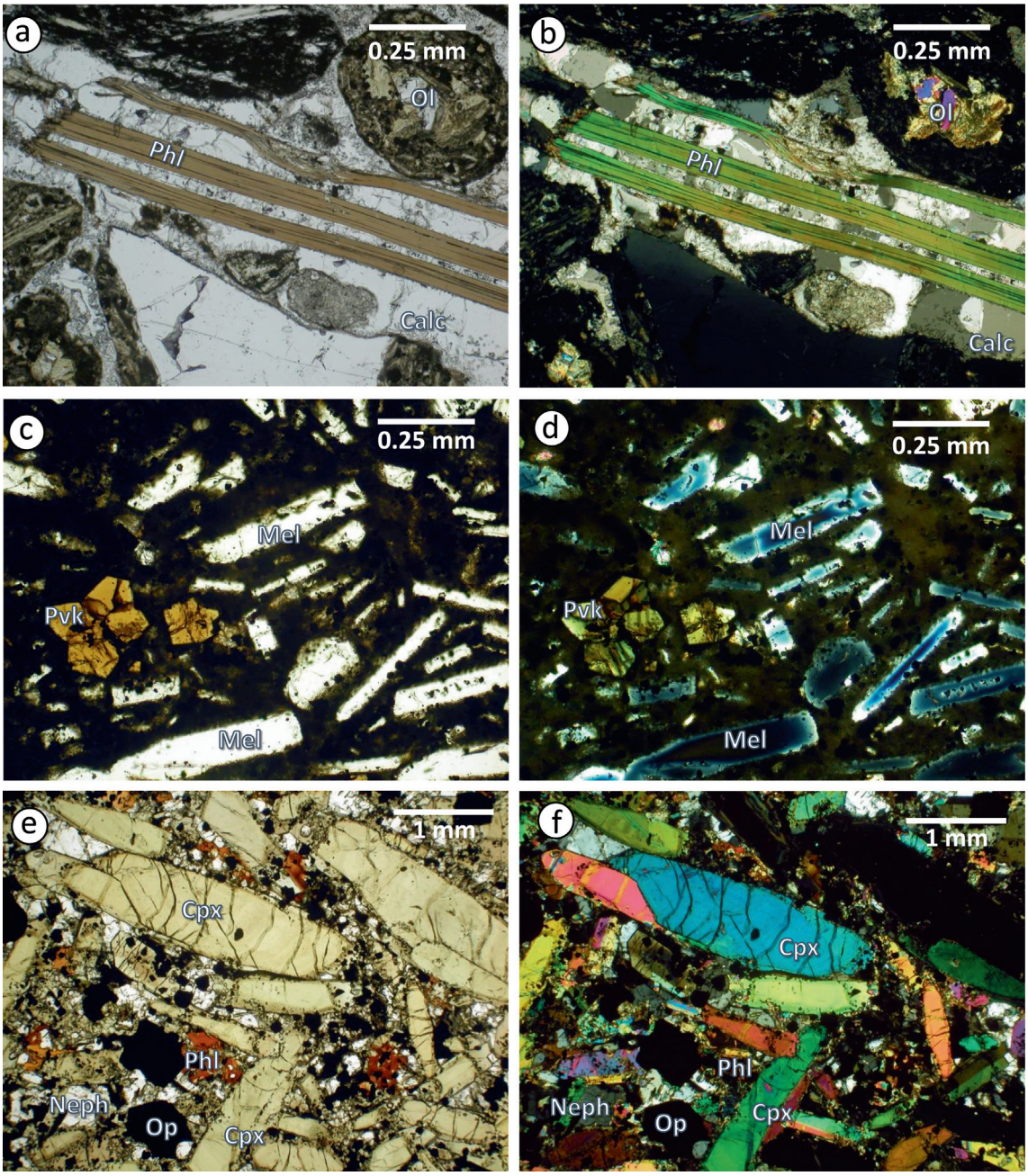

Fig. 3. Transmitted light photomicrographs of Toro Ankole thin sections: plane polarized light on the left and crossed polarized light on the right. (a) and (b) sample 91, fine/medium ash-fine lapilli tuff with matrix made of ash size particles and calcite. Matrix embeds altered lapilli with olivine and melilite phenocrysts and monocrystalline grains of phlogopite and quartz. (c) and (d) sample 90, porphyritic lava with euhedral phenocrysts of melilite and olivine plus microphenocrysts of perovskite set in a hypoyaline, hypocrystalline altered groundmass of the same phases. (e) and (f) melanocratic foidolite with euhedral to subhedral clinopyroxene and cumulate olivine. The finer matrix consists of euhedral leucite, microliths of anhedral to euhedral clinopyroxene, anhedral nepheline and kalsilite, intergranular phlogopite, rare subhedral apatite and subhedral to euhedral opaques. Calc = calcite, cpx = clinopyroxene, neph = nepheline, ol = olivine, op = opaque phases, phl = phlogopite, pvk = perovskite.

for Virunga) up to ultrapotassic (K_2O/Na_2O > 2 and up to 9 for Toro Ankole; Fig. 2b; Furman, 1995; Furman and Graham, 1999; Rosenthal et al., 2009; Foley et al., 2012; Pouclet et al., 2016; Minissale et al., 2019).

South Kivu rocks plot almost entirely in the basaltic field of the TAS diagram (44–53 wt% SiO_2; $Na_2O + K_2O$ = 2.7–5.2 wt%; Auchapt et al., 1987; Marcelot et al., 1989; Furman and Graham, 1999; Pouclet et al., 2016). The Mwenga-Kamituga and Bukavu products include quartz- and olivine-tholeiites of the pre-rift phase (from ~70 to ~7 Ma), and of younger (~8–2 Ma and ~0.014 Ma) alkali and transitional basalts, associated with more evolved types (Auchapt et al., 1987). Rungwe rocks show lower SiO_2, plotting almost entirely in the basanite/tephrite field (40–46 wt% SiO_2), with slightly higher alkali contents than South Kivu ($Na_2O + K_2O$ = 3.4–6.5; Marcelot et al., 1989; Furman, 1995).

2.2. Toro Ankole

The Toro Ankole igneous province comprises four main volcanic fields: Fort Portal, Ndale, Katwe-Kikorongo, and Bunyaruguru-Katunga (Fig. 1c; Holmes and Harwood, 1932; Foley et al., 2012; Muravyeva et al., 2014). The oldest known volcanic activity is in

the Bunyaruguru-Katunga field at 188 ka (±17.5 ka; Pitcavage et al., 2021), mainly represented by explosive, mostly phreatomagmatic, products. The most typical volcanic landforms are maars (Katwe-Kikorongo and Bunyaruguru-Katunga), monogenic craters or pyroclastic cones (Holmes and Harwood, 1937; Rosenthal et al., 2009). Lava flows are uncommon, apart from at Fort Portal, where melilite- and nepheline-bearing leucitite flows and a carbonatite lava crop out (Holmes, 1950; Barker and Nixon, 1989). Lavas have occasionally an abundant cargo of ultramafic nodules (either interpreted as mantle xenoliths or cumulate), mainly composed of clinopyroxene and Ti-rich phlogopite, with minor Ti-magnetite, titanite, apatite, perovskite and carbonate, plus rare amphibole (Lloyd, 1981; Link et al., 2008; Pitcavage et al., 2021; Innocenzi et al., 2022). No garnets or orthopyroxenes have been found in the nodule suites from Toro Ankole. Although olivine-bearing nodules are mentioned in old reports (Holmes and Harwood, 1937), this mineral is extremely rare, found as corroded and unstable single grains in biotite pyroxenites (Lloyd, 1981; Link et al., 2008), although olivine-bearing rocks were mentioned in older observations (Holmes and Harwood, 1937). The mica-pyroxenite assemblage may be the dominant paragenesis of the enriched subcontinental lithospheric mantle beneath SW Uganda (Lloyd, 1981; Pitcavage et al., 2021).

Toro Ankole volcanic rocks define two distinct clusters in the TAS diagram and, except for one sample, they define a clear compositional gap between ~22 and ~31 wt% SiO_2 (Fig. 2a). Most of the whole-rock analyses indicate moderately to strongly ultrabasic composition (SiO_2 ~ 31–46 wt%; total alkali contents mostly of 2.3–9.9 wt%). They consist of abundant melilitites, nephelinites and leucitites with minor kamafugites, picrites and basanites. The second group is represented by carbonatites with SiO_2 contents dominantly in the 11–22 wt% range. These carbonatites differ from the natrocarbonatites of Oldoinyo Lengai in the eastern rift branch (Dawson, 1989) in having very low alkali contents ($Na_2O + K_2O$ = 0.4–2.0 wt%). About 40 % of the ultrabasic rocks have potassic affinity (K_2O/Na_2O = 1.0–2.0), ~50 % are ultrapotassic (K_2O/Na_2O = 2.0–10.8), and the remaining ~10 % are of sodic to transitional affinity (K_2O/Na_2O = 0.3–0.97). Only a few whole-rock compositions of Toro Ankole rocks plot in the basic field, with 45.6–51.4 wt% of SiO_2 and 3.0–9.1 wt% total alkalies (Fig. 2a).

2.3. Virunga

The Virunga volcanic province includes, in addition to many monogenetic craters and cones, eight principal composite volcanoes, from west to east: Nyamulagira (also known as Nyamuragira), Nyiragongo, Mikeno, Karisimbi, Visoke, Sabinyo, Gahinga and Muhavura and the volcanic field of Bufumbira (Fig. 1d; Barette et al., 2017; Muravyeva et al., 2021; Minissale et al., 2022). This latter is located at the north/eastern edge of the province, slightly offset from the rift axis (Pitcavage et al., 2021). Only the eruptive centres of Nyiragongo (Minissale et al., 2019, 2022; Mafuko Nyandwi et al., 2022) and Nyamulagira (Smets et al., 2015; Boudoire et al., 2022) are considered still active (e.g., Chakrabarti et al., 2009; Minissale et al., 2019; Barrière et al., 2022). In the rest of the province, the most recent activity is Late Pleistocene (~0.2 ± 0.1 Ma; K/Ar; Guibert et al., 1975) in the central and eastern areas (Mikeno) to ~10 ± 7 ka at Karisimbi (K/Ar, De Mulder and Pasteels, 1986). Volcanic products at Virunga show less extreme compositions than those of the Toro Ankole field (Fig. 2a).

Two main suites can be identified: 1) leucite- and melilite-nephelinites, plus nepheline-leucitites (Nyiragongo, Mikeno, and Visoke; Pouclet et al., 1984; Minissale et al., 2019, 2022). Nyiragongo volcanic rocks show a SiO_2 content varying from ~32 wt % (melilitites and melilite nephelinites) to 48.4 wt% (alkali olivine basalt; Platz et al., 2004); 2) leucite basanites and SiO_2 richer compositions, up to trachytes (Nyamulagira, Karisimbi, Visoke, Sabinyo, Gahinga and Muhavura). Most of the rocks from this latter group fall in the basanite and trachybasalt fields (Fig. 2a), with minor alkali basalts and even rarer more evolved mildly alkaline compositions (Barette et al., 2017). The most evolved types occur at the Karisimbi (tephritic basanite to trachyte; Mulder et al. 1986), Gahinga (potassic trachybasalt to latite; Marcelot et al. 1989) and Sabinyo volcanoes (potassic trachybasalt to latite; Bell and Powell 1969). The $Na_2O + K_2O$ content in rocks of the Virunga Volcanic Province is highly variable with ~80 % of the products concentrated at the alkali-rich end (>5.5 wt%). The highest alkali content is recorded in the most ultrabasic Nyiragongo rocks ($Na_2O + K_2O$ up to 17.2 wt%; Demant et al. 1994; Platz et al., 2004) and the lowest (1.9 wt%) at Nyamulagira (Minissale, 2017). About half of Nyiragongo rocks are potassic (K_2O/Na_2O = 1.0–2.0) The other Virunga rock series has a potassic affinity in more than the 70 % of cases (K_2O/Na_2O = 1.0–2.0), with just a few (4 %) being ultrapotassic (K_2O/Na_2O = 2.0–6.2).

Bufumbira is distinguished by extremely variable compositions, ranging from leucitites, basanites, and olivine basalts to trachyandesites and trachytes, with clinopyroxene and olivine as the most abundant phases (Holmes and Harwood, 1937; Barifaijo et al., 2010; Pitcavage et al., 2021). The volcanic activity here is clustered in three phases: (1) ~663–110 ka in the main zones of the Bufumbira volcanic field; (2) ~56–60 ka, concentrated in the eastern corner and (3) ~23–20 ka, overlying the oldest products (Pitcavage et al., 2021). The ultrabasic and basic rocks, have $Na_2O + K_2O$ ranging between 1.3 and 11.5, and are potassic (K_2O/Na_2O = 1.04–1.63) or ultrapotassic (K_2O/Na_2O = 2.15–10.77), with strong enrichment in trace elements.

3. Results

Analytical methods are reported in Electronic Appendix 1. The results of petrographic, mineral chemical, geochemical and isotopic analyses are reported below., with further information available in Electronic Appendices 2 (detailed petrographic description), 3 (mineral chemistry) and 4 (geochemical data).

3.1. Petrography

Based on petrographic features, the Toro Ankole samples have been grouped into five main types: (1) tuffs (Fort Portal, Rusekere, Ndale, Katwe-Kikorongo and Bunyaruguru), (2) carbonatite lavas (Fort Portal and Katwe-Kikorongo), (3) silicate lavas (Bunyaruguru-Katunga and Katwe-Kikorongo), (4) ultramafic nodules (Bunyaruguru and Katwe-Kikorongo) and (5) melanocratic foidolites (Katwe-Kikorongo). The samples from Virunga (Bufumbira) province are all from lava flows.

The pyroclastic rocks are poorly-sorted, fine- to medium-grained ash and lapilli tuffs (Figs. EA1 a–d, in Electronic Appendix 2). Samples from Ndale contain abundant carbonatitic ash matrix, whereas samples from Fort Portal and Rusekere are matrix- to grain-supported lapilli tuffs, showing a heterogeneous matrix made of silicate and carbonate ash-sized particles and sparry calcite cement in which carbonatite lapilli are embedded (Figs. EA1 a–d and Figs. EA2 a–b Electronic Appendix 2). All the tuffs are rich in crustal lithics and monocrystalline grains (Fig. 3a–b). The Katwe-Kikorongo and Bunyaruguru samples differ, containing kamafugite lapilli with a hypohyaline to hypocrystalline groundmass (Figs. EA3 a–b Electronic Appendix 2).

The carbonatite lavas are hypocrystalline to holocrystalline, with porphyritic to aphanitic textures (P.I. ~ 2–20 %; Porphyritic Index = area occupied by phenocrysts over the area of the rock thin section) with phenocrysts of subhedral monticellite, resorbed

carbonates, subhedral clinopyroxene and tabular phlogopite (Figs. EA4 a–d Electronic Appendix 2). The carbonate groundmass is fine-grained and includes abundant subhedral to euhedral opaque phases, subhedral monticellite, clinopyroxene, apatite ± glass. Samples are vesicular with ~5–15 % sub-rounded vesicles (Figs. EA4 a–d Electronic Appendix 2).

The silicate lavas from Toro Ankole include kamafugites (katungites, e.g., samples 50 and 109, mafurites, e.g., sample 49, and ugandites, e.g., sample 53; see Electronic Appendix 2), olivine melilitites (samples 88 and 90 from Katunga), leucitites (samples 81, 83 and 85) and a nephelinite (114f), with P.I. ~ 10–20 %. Phenocrysts are mostly clinopyroxene, often characterized by a green core, and olivine (Figs. EA5 a–f Electronic Appendix 2) set in a hypo- to holocrystalline groundmass, which is generally optically unresolvable. Based on SEM and EMP analyses, it is made up of microliths of clinopyroxene, olivine, perovskite, kalsilite, nepheline, carbonate, opaques, minor glass ± leucite and phlogopite (Figs. EA6 a–d and Figs. EA7 a–f Electronic Appendix 2). Melilite was found as totally altered grains in sample 50 from Bunyaruguru, and as very abundant fresh phenocrysts and microphenocrysts in the olivine melilitites from Katunga (Fig. 3c and 3d).

Bufumbira (Virunga) lavas include leucite basanites and more evolved types such as leucite-bearing potassic trachybasalt and latite. They are porphyritic (P.I. ~ 20 %), with phenocrysts of olivine and clinopyroxene plus leucite microphenocrysts (Figs. EA9 a–d Electronic Appendix 2). The hypocrystalline groundmass is composed of olivine, clinopyroxene, leucite, opaques, minor glass and a variable amount of plagioclase, also found as phenocrysts in samples 156 and 159.

The ultramafic nodules are fine- to medium-grained holocrystalline, with clinopyroxenite to glimmerite compositions, plus minor amounts of perovskite, opaques and calcite as patches and fracture filling (Figs. EA10 a–f Electronic Appendix 2).

The melanocratic foidolites comprise medium to coarse-grained holocrystalline melteigites (samples 84 and 126) and one missourite (sample 80). They consist of clinopyroxene (~60 % in samples 80 and 84 and 40–50 % in 126), iddingsitised olivine (~15 % modal) and magnetite (5–10 % modal; Fig. 3e–f). The intergranular matrix is made of leucite (the predominant foid in missourite sample 80), microliths of clinopyroxene, nepheline (more abundant, up to 30 % modal in melteigites 84 and 126), phlogopite, perovskite, apatite and opaques (Figs. EA11 a–d Electronic Appendix 2).

3.2. Mineral and glass chemistry

All the EMP results, including chemical compositions of the main mineral phases are reported in Electronic Appendices 3a and 3b.

Olivine is roughly uniform in composition in all Toro Ankole lavas, with forsterite component [Fo = 100 * Mg/(Mg + Fe)] generally ranging from 80 to 90 mol % (Fig. 4a), and a large overlap among phenocryst cores (Fo_{80-90}) and rims, microphenocrysts and groundmass (Fo_{81-88}). Bufumbira olivine shows more variable Fo content (Fo_{60-88}). The carbonatite sample contains no olivine but monticellite (Fo_{39-43}-Fa_{4-9}-La_{48-56}-Tp_{1-2}; Fig. 4a) with Mg# varying between 0.78 and 0.92 and CaO ranging from 34.14 to 38.46 wt%.

Clinopyroxene analyses cluster in the diopside field (Morimoto, 1989), except for a few crystals from Bunyaruguru tuffs that are enriched in Na and Fe^{3+}, often showing Ca excess (CaO = 18.33–26.12 wt%; Fig. 4b). Clinopyroxene from an ultramafic nodule from Bunyaruguru is slightly richer in Fe ($En_{45}Fs_7Wo_{48}$). Toro Ankole phenocryst cores have high Mg# [Mg# 0.74–0.99; Mg/(Mg + Fe^{2+})], with >50 % of the analyses showing Mg# >0.90. These compositions overlap with those of phenocryst rims and groundmass phases (Mg# 0.88–0.99). SiO_2 (45.86–54.07 wt%) and Al_2O_3 (0.00–5.11 wt%) do not always sum up to 2 apfu, and up to 0.079 apfu of $^{IV}Fe^{3+}$ is allocated to fill the tetrahedral site.

Brown mica has been classified (Mica$^+$ software; Yavuz, 2003) as phlogopite and ferroan phlogopite, with Mg# ranging from 0.82 (in carbonatite and in lava groundmass) to 0.97 (in monocrystalline grains in tuffs; Fig. 4c). Except for micas from carbonatite, Si + ^{IV}Al is generally <4 apfu: the tetrahedral deficiency becomes appreciable for micas in melanocratic foidolite (melteigite) and in Bunyaruguru lavas, especially in rims and groundmass. In these samples, the tetrahedral deficiency is compensated by Fe^{3+} (up to 0.345 apfu Fe^{3+}). TiO_2 contents are high, varying between 4.78 and 7.77 wt%, with the lowest values found in carbonatites and highest in lava groundmass. The lower titanium in phlogopite from carbonatite samples may be related to the concomitant crystallization of Ti-magnetite. Barium is low in phlogopite in carbonatites, ultramafic nodules and monocrystalline grains in tuffs, whereas it increases with differentiation in the lavas and in the foidolite up to 3.78 wt% BaO. Fluorine reaches the highest values in micas in the ultramafic nodules (up to 3.41 wt%) and groundmass phases (up to 4.30 wt%).

Fresh melilite is only found in one sample from Toro Ankole, showing a high MgO content (10.25–10.64 wt%), with low Na_2O (1.69–2.68 wt%) and FeO (2.87–3.44 wt%, Fe^{3+} = 0.049–0.115 apfu Fe^{3+} and Fe^{2+} = 0.035–0.062 apfu Fe^{2+}). Al_2O_3 (2.70–3.55 wt%) partially occupies the tetrahedral site (^{T2}Al = 0.005–0.037 and ^{T1}Al = 0.127–0.154 apfu Al).

Nepheline is found in the groundmass of leucitite sample 81 and as an intergranular phase in the melanocratic foidolite 126 (melteigite, both from Katwe-Kikorongo; Fig. 4d). It shows a Ne# ranging between 2.60 and 3.16 [100 * Ne/(Ks + Ne + Sil)] where Ks = k, Ne = Na and Sil = Si-(2 * Ca + Na + K)]. The variable amounts of K_2O (6.43–8.61 wt%) and fairly uniform Na_2O (14.66–15.22 wt%) plot far from the known solvus curve between kalsilite and nepheline.

Leucite occurs as microphenocrysts in the groundmass of Toro Ankole (both Bunyaruguru and Katwe-Kikorongo) and Virunga (Bufumbira) samples (Fig. 4d). It is found in the melanocratic foidolite (melteigite) sample (126) and lavas (53, 109, 159 and 169). FeO (0.26–0.68 wt%) and CaO (<0.11 wt%) are always very low, except for leucite in Toro Ankole kamafugite 109 (FeO = 1.95 wt%; CaO = 0.63 wt%) and 53 (FeO = 1.04–1.62 wt% and CaO = 0.00–0.16 wt%). Leucite shows almost pure composition, with K# [100 * K/(K + Na)] ranging from 97.1 to 99.9.

Kalsilite occurs as a relatively common groundmass phase (>5–10 % modal abundance) in many lavas and lapilli tuffs from Toro Ankole (Bunyaruguru and Katwe-Kikorongo; Fig. 4d). The composition varies over a relatively narrow range with Kal [100 * Ks/(Ks + Ne + Sil)] of 80–93. Again, the data do not cross the solvus curve between kalsilite and nepheline, highlighting the primary nature of kalsilite in Toro Ankole products.

All carbonates are mainly calcite (Fig. 4e). Primary carbonates have been identified in carbonatite and kamafugite lavas, as groundmass phases. The first ones show MgO < 2.37 wt%, SrO < 1.01 wt% and BaO < 1.89 wt%, whereas carbonate in kamafugites groundmass has MgO < 4.20 wt%, SrO < 4.87 wt% and BaO < 4.00 wt%. Primary carbonate is also hosted in lapilli, as intergranular phases and euhedral laths, exhibiting a calcite composition, with a variable enrichment in SrO (highlighted by SEM-EDS analyses). Compared to primary carbonate, the secondary sparry calcite cementing the lapilli in some tuffs has much lower SrO content coupled with a slightly higher MgO, as revealed by SEM-EDS analyses.

Spurrite, $Ca_5(SiO_4)_2(CO_3)$, has been found as a common groundmass phase in the carbonatite lava from Fort Portal. It shows relatively high P_2O_5 (3.77–4.15 wt%) and Na_2O, contents (2.14–2.41 wt%).

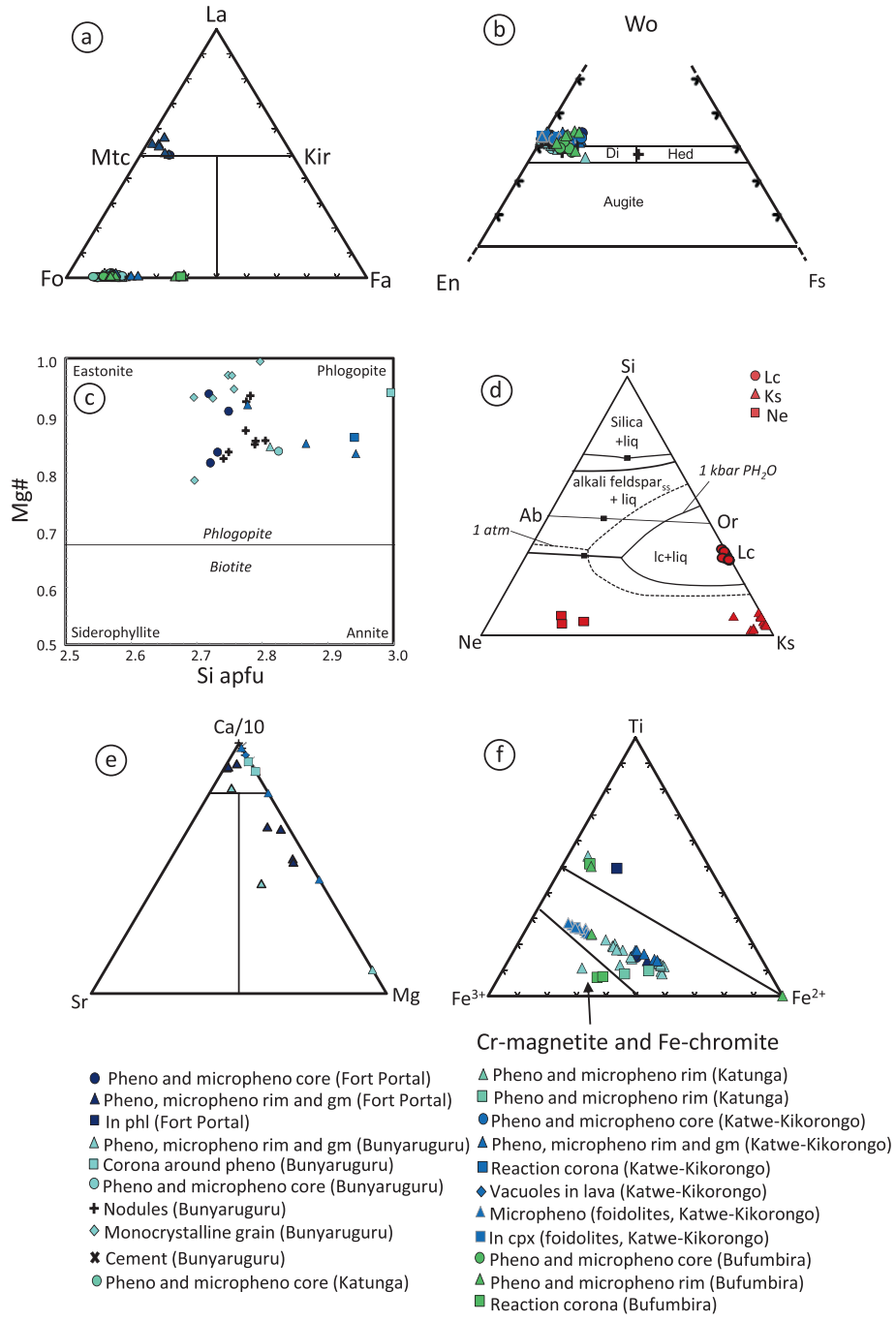

Fig. 4. (a) Forsterite-Fayalite-Larnite ternary diagram for olivine in the volcanic products from Toro Ankole and Bufumbira. (b): Wollastonite-Enstatite-Ferrosilite ternary diagram for clinopyroxene of the volcanic products from Toro Ankole and Bufumbira fields (from Morimoto, 1988). (c) Si (apfu)-Mg# diagram for brown mica of the volcanic products from Toro Ankole and Bufumbira. (d) Petrogenetic system for foids: silica-nepheline-kalsilite triangle diagram of the volcanic products from Toro Ankole and Bufumbira. (e) Ca/10-Sr-Mg (apfu) ternary diagram for the carbonate of the volcanic products from Toro Ankole. (f): Ti-Fe^{3+}-Fe^{2+} (apfu) ternary diagram for the opaque phases of the volcanic products from Toro Ankole and Bufumbira.

Opaque minerals (Fig. 4f) belong mostly to the spinel solid solutions (FeO_{tot} = 32.58–77.53 wt%, Fe^{3+} = 1.992–1.433 and Fe^{2+} = 0.000–1.014) and subordinately to the rhombohedral phases solid solutions (with much higher TiO_2, 45.66–52.07 wt%). These minerals occur as groundmass phases or microphenocrysts and as inclusions in phlogopite and olivine phenocrysts. On average, Cr_2O_3 is not very high (0.00–5.96 wt), with the exception of Cr-magnetite and ferrian chromite (Gargiulo et al., 2013) enclosed in olivine phenocrysts and in the groundmass of two lava samples from Bunyaruguru (kamafugite 57) and Katunga (olivine melilitite 90), which have Cr_2O_3 up to 41.64 wt%.

Perovskite is found in the groundmass and as microphenocrysts in both lavas and lapilli of Bunyaruguru and Katwe-Kikorongo (Toro Ankole), and as accessory phase in the ultramafic nodules. It exhibits a uniform composition with low FeO (0.71–1.71 wt%; only one microphenocryst in Katwe-Kikorongo lapilli shows a higher FeO of 4.25 wt%). BaO is always below the detection limit and SrO varies in the range 0.00–1.33 wt%.

3.3. Whole-rock geochemistry

Representative bulk-rock major oxides compositions of the studied rocks are shown in Table 1 (Toro Ankole) and Table 2 (Virunga), whereas trace element values are reported in Table 3 (Toro Ankole) and Table 4 (Virunga). All data can be found in Electronic Appendix 5.

3.3.1. Major oxides

Major oxide contents allow an easy distinction within Toro-Ankole lavas and tuffs, among carbonatites and silico-carbonatites from moderately ultrabasic rocks (Fig. 5 and Electronic Appendix 5). Carbonatite and silico-carbonatite lavas (samples 16, 17 and 79) and tuffs (samples 11, 34, 35 and 128) are characterized by very low SiO_2 (4.89–21.78 wt%), and low alkali contents (Na_2O + K_2O = 0.44–2.03 wt%). Carbonatites have CaO between 25.17 and 47.57 wt%, with CO_2 ranging from 11.50 to 32.40 wt%. The difference between measured LOI and the amount of CO_2 varies from 4.25 to 9.06 wt%, probably highlighting presence of H_2O. Within the carbonatite group, Fort Portal samples are also enriched in MgO (up to 8.76 wt%), Fe_2O_{3tot} (up to 13.68 wt%), and P_2O_5 (up to 3.59 wt%). On the other hand, moderately ultrabasic rocks, mostly falling in the foidite field, have higher SiO_2 (36.35–42.03 wt%) and higher total alkali contents (4.05 to 8.32 wt%; Fig. 2a). They are variably enriched in K_2O (0.67–7.15 wt%), belonging to potassic and ultrapotassic series (All Bunyaruguru samples, sample 88 from Katunga and sample 114 from Katwe-Kikorongo are ultrapotassic; Fig. 2b).

The moderately ultrabasic rocks show variable MgO contents (6.08–22.2 wt%), with the MgO-richest samples being characterized by abundant olivine and clinopyroxene phenocrysts as well as ultramafic and phlogopite-rich nodules. One Toro Ankole lava (sample 110), although plagioclase-free, plots in the basalt field in the TAS diagram. The presence of secondary zeolites in the groundmass probably indicates post-emplacement modification of the original composition.

The few lavas from Virunga (basanite, trachybasalt and trachyandesite), define a mildly alkaline evolutionary trend (Fig. 2a), with increasing total alkalies (Na_2O + K_2O up to 7.98 wt%) coupled with an increase in SiO_2 (up to 56.97 wt%).

Two of the three ultramafic nodules are ultrabasic (SiO_2 = 33.86–35.02 wt%), whereas sample 65 has higher SiO_2 (46.58 wt%), reflecting higher modal clinopyroxene. Total alkali content ranges from 2.35 to 8.89 wt%, with K_2O (up to 8.66 wt%) always much higher than Na_2O (0.32–0.88 wt%). They are also characterized by high MgO (14.59–19.03 wt%) and Fe_2O_{3tot} (8.46–14.11 wt%). The high TiO_2 amount of sample 86 (9.19 wt%) is due to the high modal content of opaque phases. Melanocratic foidolites are

Table 1
Representative whole rock major elements compositions of volcanic products from the WEAR, Toro Ankole Volcanic Province (N' Fort Portal, Rusekere, Ndale, Bunyaruguru, K-K = Katwe-Kikorongo, Katunga).

Sample	Locality	Rock Type	SiO_2	TiO_2	Al_2O_3	Fe_2O_3	MnO	MgO	CaO	Na_2O	K_2O	P_2O_5	L.O.I.	CO_2	Total	Mg#
11	N' Fort Portal	Carbonatitic tuff	21.57	1.92	6.00	0.69	0.32	5.80	25.38	0.80	1.04	2.41	21.03	15.20	97.95	0.54
16	N' Fort Portal	Carbonatite Lava	12.37	1.83	3.15	13.68	0.48	8.61	30.07	0.19	0.25	3.59	23.44	16.60	97.65	0.59
17	N' Fort Portal	Carbonatite Lava	16.90	2.08	4.20	13.22	0.42	8.76	31.76	0.67	0.33	3.20	16.32	11.50	97.86	0.61
34	Ruskere	Carbonatitic tuff	19.47	2.02	5.56	9.65	0.27	6.97	25.17	0.52	1.13	2.03	25.06	16.00	97.84	0.63
35	Ruskere	Carbonatitic tuff	14.40	1.94	4.76	10.65	0.35	7.06	29.38	0.44	0.57	2.69	24.62	19.50	96.85	0.61
47	Bunyaruguru	Kamafugite lava	39.88	4.49	7.86	12.17	0.21	9.40	14.15	1.50	3.99	1.21	4.83	0.27	99.69	0.64
49	Bunyaruguru	Kamafugite lava	37.06	5.30	6.70	12.23	0.19	11.68	13.20	0.78	7.05	1.15	2.43	0.52	97.77	0.69
51	Bunyaruguru	Kamafugite lava	36.35	4.39	7.71	11.68	0.19	10.57	14.26	1.43	6.02	1.57	4.77	1.67	98.95	0.68
53	Bunyaruguru	Kamafugite lava	40.03	5.32	7.30	12.02	0.18	12.94	11.31	1.04	6.13	0.43	2.40		99.09	0.72
55	Bunyaruguru	Kamafugite lava	42.03	3.97	5.97	12.12	0.15	22.20	6.82	0.82	4.85	0.15	0.72	0.06	99.81	0.81
57	Bunyaruguru	Kamafugite lava	40.52	5.24	6.72	11.51	0.15	17.78	8.98	1.17	7.15	0.09	0.20	0.06	99.51	0.78
58	Bunyaruguru	Kamafugite lava	40.05	5.50	6.85	11.67	0.16	15.21	10.02	0.68	5.30	0.30	3.69	0.06	99.43	0.75
70	Bunyaruguru	Tuff	43.70	3.20	6.19	9.36	0.17	10.34	8.51	0.22	2.90	0.94	13.62	31.60	99.15	0.72
65	Bunyaruguru	Ultramafic nodule	46.58	2.58	5.57	8.46	0.10	14.59	17.50	0.68	2.71	0.01	1.01	0.70	99.79	0.80
79	K-K	Carbonatite lava	4.89	0.34	1.25	4.10	0.30	0.73	47.57	0.09	0.42	1.94	34.57	3.24	96.19	0.29
81	K-K	Leucitite lava	39.84	5.23	9.17	13.84	0.22	6.41	12.79	2.26	4.03	1.07	4.65	1.13	99.51	0.52
83	K-K	Leucitite lava	39.76	5.60	9.64	12.90	0.22	6.45	14.46	2.26	4.07	1.04	3.26	0.89	99.66	0.54
85	K-K	Leucitite lava	40.54	5.79	9.39	13.56	0.22	6.76	13.94	2.51	4.50	0.88	1.36	0.19	99.44	0.54
107	Congo road	Tuff	35.95	4.59	6.00	12.49	0.21	12.71	17.28	1.14	3.83	0.96	3.38	0.24	98.54	0.70
109	Congo road	Kamafugite lava	40.05	3.55	8.70	10.62	0.17	6.08	12.18	1.46	2.59	0.94	13.79	6.73	100.13	0.57
110	K-K	Lava	50.91	1.43	12.61	15.98	0.23	5.00	9.26	2.30	0.67	0.18	0.27		98.84	0.42
114f	K-K	Nephelinite lava	35.08	6.25	6.45	14.65	0.22	9.37	11.94	1.59	3.76	1.22	8.38	3.19	98.91	0.60
86	K-K	Ultramafic nodule	33.86	9.19	12.33	14.11	0.10	17.06	1.83	0.32	8.66	0.15	0.47	0.03	98.08	0.74
95	K-K	Ultramafic nodule	35.02	3.69	6.49	11.89	0.21	19.03	9.73	0.60	1.75	0.85	10.38	1.26	99.64	0.79
84	K-K	Foidolite	41.08	4.93	6.45	14.67	0.18	11.03	16.21	1.39	2.69	0.43	0.82	0.58	99.88	0.64
80	K-K	Foidolite	42.28	4.72	8.72	13.52	0.19	9.31	13.98	1.16	2.76	0.60	2.23	0.15	99.46	0.62
126	K-K	Foidolite	37.26	6.02	8.60	14.51	0.25	6.74	15.30	2.66	3.02	1.43	4.21	0.95	100.00	0.52
88	Katunga	Ol melilitite lava	38.76	5.92	7.71	14.33	0.20	10.56	15.46	1.87	3.87	0.90	0.58	0.03	100.16	0.63
90	Katunga	Ol melilitite lava	41.91	4.94	8.87	13.59	0.19	9.17	13.14	2.33	4.21	0.56	−0.08	0.09	98.82	0.61
128	Ndale	Carbonatitic tuff	21.78	0.44	6.22	5.61	0.12	3.64	30.25	0.90	1.13	1.23	26.35	22.10	97.67	0.60

Table 2
Representative whole rock major elements compositions of volcanic products from the WEAR, Virunga Volcanic Province (Bufumbira).

Sample	Locality	Rock Type	SiO_2	TiO_2	Al_2O_3	Fe_2O_3	MnO	MgO	CaO	Na_2O	K_2O	P_2O_5	L.O.I.	CO_2	Total	Mg#
156	Bufumbira	Trachyandesite lava	56.97	2.29	15.54	8.46	0.12	3.30	5.42	3.25	4.73	0.47	−0.23	0.05	100.32	0.48
159	Bufumbira	Trachybasalt lava	48.84	2.94	14.21	11.74	0.18	6.38	8.66	2.89	4.07	0.62	−0.58	0.04	99.95	0.56
169	Bufumbira	Basanite Lava	43.54	2.76	8.79	12.03	0.17	17.29	10.99	1.68	2.74	0.42	−0.38	0.11	100.03	0.77
171	Bufumbira	Basanite Lava	44.86	2.78	12.15	12.37	0.18	12.65	9.65	1.78	2.66	0.60	0.47	0.02	100.15	0.70

Table 3
Representative whole rock trace elements compositions of volcanic products from the WEAR, Toro Ankole Volcanic Province (N' Fort Portal, Rusekere, Ndale, Bunyaruguru, K-K = Katwe-Kikorongo, Katunga).

Sample	Locality	Rock Type	Rb	Sr	Ba	Cs	Sc	V	Cr	Co	Ni	Cu	Zn	Y	Zr	Nb	Hf	Ta
11	N' Fort Portal	Carbonatitic tuff	35	4623	2571	0.9	16	267	90	30	20	50	150	36	150	165	3.1	8.1
16	N' Fort Portal	Carbonatite Lava	6	3329	4184		14	365	50	28	30	40	220	58	628	461	9.2	20
17	N' Fort Portal	Carbonatite Lava	7	5023	2322	0.6	15	347	80	33		50	170	50	226	157	3.1	5.2
34	Ruskere	Carbonatitic tuff	26	3916	1752	0.7	13	204	80	28		50	110	34	285	153	4.4	5.8
35	Ruskere	Carbonatitic tuff	11	7734	6287		13	245	60	28		50	130	44	225	149	3.1	4.2
47	Bunyaruguru	Kamafugite lava	90	2699	2201		26	151	230	50	40	170	120	17	435	286	9.8	19
49	Bunyaruguru	Kamafugite lava	166	2543	2789	0.6	25	220	610	56	120	150	100	15	436	251	9.6	17
51	Bunyaruguru	Kamafugite lava	125	3307	2331		23	220	210	47	50	140	100	16	376	280	8.9	18
53	Bunyaruguru	Kamafugite lava	158	2182	2219	0.5	22	251	1000	62	240	130	90	13	374	200	8.5	13
55	Bunyaruguru	Kamafugite lava	192	585	976	0.6	17	164	1550	99	1020	90	80	6	154	81	4.1	6.7
57	Bunyaruguru	Kamafugite lava	141	1129	1516		21	200	1240	78	560	100	80	9	264	136	6.3	9.9
58	Bunyaruguru	Kamafugite lava	170	1409	2753	0.6	21	177	1070	75	470	110	90	9	322	170	8.1	12
70	Bunyaruguru	Tuff	99	1201	1496	0.7	23	75	310	41	60	120	70	15	354	207	7.4	12
65	Bunyaruguru	Ultramafic nodule	74	333	795		57	171	370	48	100	10	30	3	93	16	3	1.4
79	K-K	Carbonatite lava	9	6747	12280			332				20	130	15	59	293	0.9	1.1
81	K-K	Leucitite lava	116	2381	1310	1.2	19	422	220	49		170	110	19	481	280	9.6	15
83	K-K	Leucitite lava	124	2333	2659	1.3	21	514	40	42		190	100	18	472	243	9.4	16
85	K-K	Leucitite lava	123	2026	1769	1.3	24	571	90	46		180	100	17	382	236	9.3	17
107	congo road	Tuff	122	2737	2131	0.7	25	158	580	55	190	150	100	16	349	254	7.6	14
109	congo road	Kamafugite lava	98	2410	1231	1.2	18	280	170	34		100	100	21	378	176	8.6	11
110	K-K	Lava	20	191	312	0.6	46	415	40	51		20	130	27	113	12	2.7	0.6
114f	K-K	Nephelinite lava	102	1409	1087	1	27	401	340	54	40	140	100	18	444	232	9.8	15
86	K-K	Ultramafic nodule	243	335	2851	1.6	18	287	120	103	60	40	50	1	104	62	2.5	5.3
95	K-K	Ultramafic nodule	55	2811	2359	0.8	22	96	560	60	380	120	100	15	327	245	7.1	12
84	K-K	Foidolite	76	1151	881	0.7	46	378	530	64	80	110	80	9	251	111	5.9	7.7
80	K-K	Foidolite	129	1413	3647	1.2	32	396	480	58	80	110	90	13	261	136	6.7	10
126	K-K	Foidolite	79	2840	1792	1.4	18	565		46		230	110	20	427	275	9.8	16
88	Katunga	Ol melilitite lava	79	2492	851		33	420	470	61	80	150	100	16	340	211	8.3	14
90	Katunga	Ol melilitite lava	108	1378	1461	1	33	390	460	55	70	140	90	13	292	153	6.9	10
128	Ndale	Carbonatitic tuff	41	2436	6613	0.8	19	157	70	13	40	40	50	22	143	128	2.8	4

Sample	La	Ce	Pr	Nd	Sm	Eu	Gd	Tb	Dy	Ho	Er	Tm	Yb	Lu	Pb	Th	U	Ga
11	337	626	69.4	241	33.5	8.15	17.5	2	9.4	1.4	3.3	0.4	2.3	0.36	20	38	9.9	15
16	593	1080	117	413	56.8	12.6	31.7	3.7	16.3	2.5	5.6	0.67	3.8	0.55	27	66.3	16.7	16
17	473	886	97.4	342	45.9	11.6	24.6	2.8	12.6	1.9	4.4	0.52	2.9	0.44	17	52.5	13.7	16
34	294	555	60.8	215	29.2	6.93	15.7	1.8	8.1	1.3	2.8	0.36	2	0.31	16	29.9	9.1	14
35	398	742	84	291	38.8	9.4	21.2	2.3	10.8	1.7	3.7	0.45	2.6	0.37	18	41.7	12	14
47	262	503	55.6	192	24.3	5.77	11.4	1.2	5.1	0.7	1.7	0.2	1.1	0.18	9	33.8	7.5	17
49	229	444	48.8	172	22.5	5.24	10.4	1.1	4.5	0.6	1.3	0.16	0.9	0.14	9	27	6.5	16
51	234	455	51	177	22.7	5.31	10.7	1.1	4.8	0.7	1.5	0.19	1.1	0.17		31	7.5	17
53	168	333	37.5	133	17.7	4.35	8.5	0.9	3.7	0.5	1.1	0.14	0.8	0.12	7	19.3	4.5	15
55	66.1	129	14.5	51	6.7	1.68	3.5	0.4	1.8	0.3	0.7	0.08	0.5	0.08		8	1.8	12
57	112	222	25	88.4	12	2.91	5.9	0.6	2.8	0.4	0.8	0.1	0.6	0.09		11.7	3	14
58	137	266	30	106	13.8	3.39	6.8	0.7	3	0.4	0.9	0.12	0.7	0.09		15	3.9	14
70	219	418	45.6	156	19.7	4.54	9.2	0.9	4.2	0.6	1.5	0.19	1.2	0.17	11	25.5	6.1	14
65	8.9	29	4.46	19.8	3.5	0.88	1.8	0.2	0.9	0.1	0.3		0.2	0.04		0.2		9
79	339	428	37.7	107	11.8	2.49	5.8	0.6	2.9	0.5	1.2	0.16	0.9	0.14	25	4.4	6.5	6
81	222	425	47.3	165	22.1	5.22	11	1.3	5.3	0.8	1.8	0.23	1.3	0.19	11	27.9	7	20
83	190	377	42.7	152	20.1	4.8	10.2	1.1	5	0.7	1.7	0.21	1.2	0.18	10	24.6	6.9	21
85	195	393	45.4	160	21	4.91	10.4	1.1	4.9	0.8	1.7	0.21	1.2	0.18	9	26.1	5.8	22
107	236	465	52.4	181	22.8	5.25	10.4	1.1	4.5	0.6	1.4	0.17	1	0.15	8	29.8	7	14
109	154	307	35.3	123	16.8	4	9.3	1.1	5.3	0.9	2.2	0.29	1.7	0.28	11	21	4.4	19
110	14.3	31.6	4.12	17.8	4.2	1.17	4.1	0.7	4.9	1	3.2	0.46	3.2	0.49		1.9	0.5	17
114f	192	380	44.1	158	21.6	5.14	11.1	1.2	5.3	0.8	1.6	0.21	1.1	0.15	8	21.3	4.7	18
86	11.4	17.6	1.79	6.1	1	0.23	0.6		0.4		0.2		0.2	0.03		0.5	0.4	21
95	241	456	51.4	177	21.9	5.05	10	1	4.5	0.6	1.4	0.18	1	0.17	9	31.1	6.9	13
84	89.3	183	21.8	79.9	11.3	2.69	5.7	0.6	2.8	0.4	0.9	0.12	0.7	0.1		10.5	2.5	17
80	126	270	29.4	106	14.3	3.32	7.2	0.8	3.6	0.6	1.3	0.17	1	0.15	7	14.8	1.5	18
126	196	364	40.2	141	19.6	4.72	10.2	1.2	5.3	0.8	1.8	0.22	1.3	0.19	10	20.3	6.3	21
88	166	329	38	137	18.9	4.56	9.5	1	4.7	0.7	1.6	0.19	1.2	0.16		19	4.7	18
90	125	253	29.2	104	14.1	3.36	7.3	0.8	3.7	0.6	1.3	0.17	1	0.16	7	16.2	1.5	19
128	151	272	29.7	103	14.1	3.22	8	1	5.2	0.8	2	0.27	1.7	0.26	12	24.2	7.7	10

ultrabasic (SiO_2 = 37.24–42.28 wt%), with total alkalis ranging from 3.92 to 5.67 wt% (K_2O always higher than Na_2O).

3.3.2. Trace elements

Toro Ankole carbonatites are characterized by the strongest enrichment of incompatible trace elements, compared to the moderately ultrabasic group and melanocratic foidolites (Fig. 6). Notably, carbonatite lavas show lower Rb, but higher Sr, Ba, REE, Pb, Th and U than the moderately ultrabasic group. The incompatible element range of Toro Ankole carbonatites (Fig. 7a and 8a) resembles the average composition of worldwide Ca-carbonatites (Rb = 14 ppm, Sr = 7272 ppm, Ba = 3044 ppm, Nb = 343 ppm,

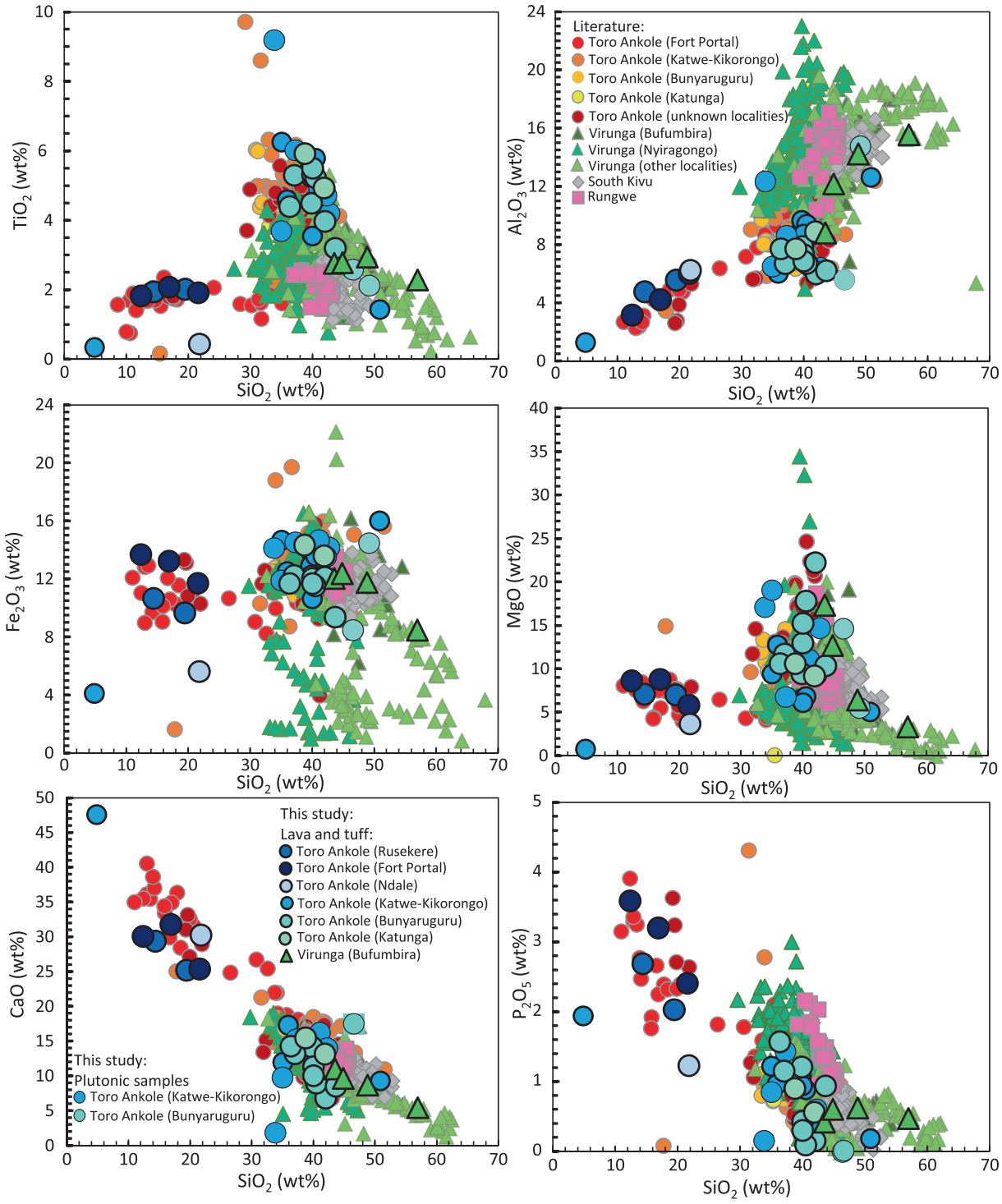

Fig. 5. Harker diagrams for TiO_2, Al_2O_3, Fe_2O_3, MgO, CaO and P_2O_5 vs silica. Strongly ultrabasic samples are from Rusekere (tuffs 34 and 35), Fort Portal (lavas 16 and 17 and tuff 11), Ndale (sample 128) and from Katwe-Kikorongo (lava 79 and tuff 107). Moderately ultrabasic/basic lavas from Bunyaruguru (47, 49, 51, 53, 55, 57 and 58), from Katwe-Kikorongo (81, 83, 85, 109, 110 and 114f) and Katunga (88 and 90), Bufumbira lavas (156, 159, 169 and 171), melanocratic foidolites from Katwe-Kikorongo (80, 84 and 126), ultramafic nodules from Bunyaruguru (65) and Katwe-Kikorongo (86 and 95) are plotted. Literature data are also reported for comparison.

Ta = 4.9 ppm, ΣREE = 3731 ppm; Woolley and Kempe, 1989; Chakhmouradian, 2006). No regular variation is registered among incompatible elements with SiO_2 increases from ~4.9 to 21.8 wt%. Except for the CaO-richest (47.6 wt%) sample, the Toro Ankole carbonatites show a poorly defined negative trend of REE abundance with SiO_2.

Virunga samples, both form this study and literature data, define cloudier variations of trace elements with SiO_2, suggesting the existence of independent magma plumbing systems in the various volcanic fields, with Nyiragongo typically showing higher Sr-Ba, Nb-Ta and REE than the other Virunga volcanoes. The new data for Virunga show positive trends for LILE (with the exception of Sr), REE Pb, Th and U, and negative correlation for TE with SiO_2 (Fig. 6).

Primitive mantle-normalized incompatible elements of Toro Ankole show spiky patterns (Fig. 7a–c and Electronic Appendix 5). Among the carbonatite rocks, the lavas show more pronounced inter-elemental fractionation than tuffs. Deep troughs are observed for Rb, K, Zr, Hf and Ti, with less marked negative anomalies for Pb,

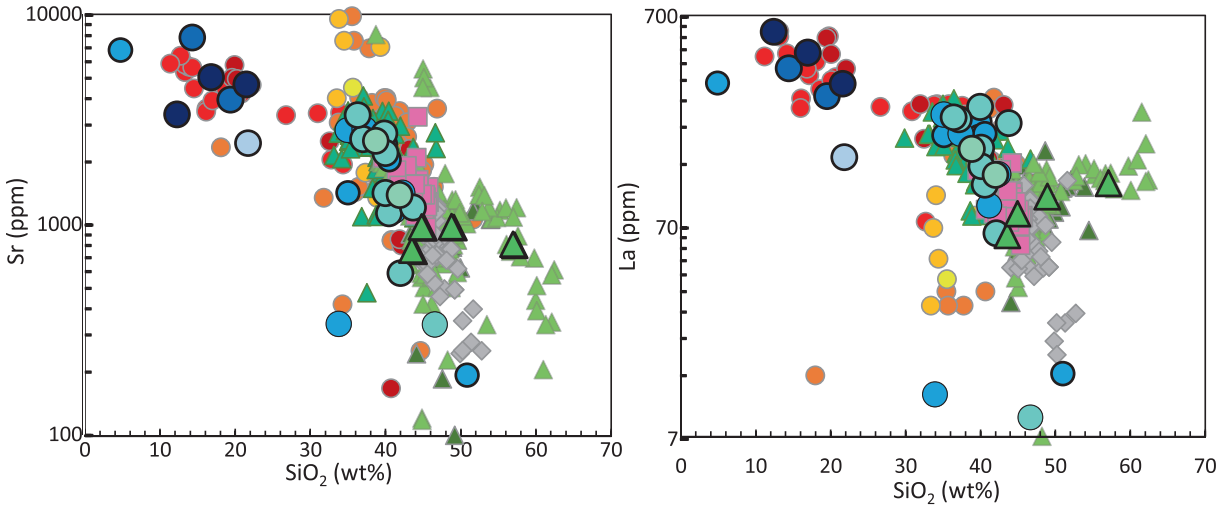

Fig. 6. Sr and La vs silica. Samples as in Fig. 5, symbols and literature data as in Fig. 2a.

and the Nb-Ta pair is decoupled (more enriched) from the Hf-Zr pair. The carbonatite tuffs (Electronic Appendix 5) mimic the overall pattern of the lavas, due to the abundance of carbonate lapilli and primary carbonate matrix (Fig. 7a), however, some tuffs are slightly depleted probably due to a dilution caused by the presence of crustal xenoliths, but also due to the presence of secondary carbonate cement. Carbonatite lava 79 from Katwe-Kikorongo, characterized by the lowest SiO_2 and highest CaO, defines a pattern resembling that of the other carbonatite, but displaced towards much lower incompatible element contents, with the exception of Ba and Sr.

The moderately ultrabasic rocks describe a uniform pattern characterized by fewer troughs and peaks than the carbonatites, albeit with similar overall abundances (Fig. 7b). Their patterns show slight negative anomalies at K, Pb and P, and less marked spikes for U and Y. Lava sample 110, with the highest SiO_2 content, exhibits a distinct trend shifted towards lower incompatible element contents. Virunga lavas share many characteristics with the moderately ultrabasic Toro Ankole group, but with smoother anomalies and lower overall incompatible element contents. Only HREE are more enriched and less fractionated in Virunga than Toro Ankole rocks.

Toro Ankole melanocratic foidolites define a pattern comparable with that of the moderately ultrabasic rocks highlighting their more evolved nature. Among ultramafic nodules, sample 65 has negative anomalies at Th, P and U, whereas Pb is below the detection limit (Electronic Appendix 5). Potassium and Ti show positive peaks. Sample 86 has negative anomalies at Th, Sm and Y, with Pb again below the detection limit, and positive peaks for Sr, Zr, Hf and Ti. Positive peaks for K and Ti indicate the abundance of phlogopite and opaques, probably Ti-magnetite, in the nodules. Sample 95 is more enriched and displays a less fractionated pattern with negative spikes at Rb, K and Pb, probably due to a higher content of clinopyroxene and perovskite and a lower amount of modal phlogopite.

Rare Earth Elements have been normalised to CI chondrite (Fig. 8a–c and Electronic Appendix 5). The strongly to moderately ultrabasic samples and melanocratic foidolites from Toro Ankole, as well as Virunga lavas, show similar patterns with no anomalies at Eu and Ce. All the samples show strong REE fractionation which increases with decreasing SiO_2. Albeit showing very similar patterns, the carbonatite lavas from Fort Portal have REE content higher than that of carbonatite tuffs (Fig. 8).

Virunga lavas are less enriched in light REE but exhibit similar LREE fractionation [$(La/Sm)_N \sim 9–11$ for Toro Ankole samples and ~8–9 for Virunga lavas]. HREE are slightly more enriched and less fractionated [average $Lu_N \sim 8.8$ for Virunga vs. 5.1 for Toro Ankole; $(La/Lu)_N \sim 31–37$ for Virunga vs. 57–169 for Toro Ankole; Fig. 8c].

3.4. Isotope geochemistry (Sr-Nd-Pb-B)

Radiogenic (Sr-Nd-Pb) and stable (B) isotopic ratios have been analysed for twelve representative samples: three carbonatite lavas (samples 16, 17 and 79) and four moderately ultrabasic lavas (sample 55, 85, 90, 110) from Toro Ankole, ultramafic nodules (samples 65, 86 and 95), and two Virunga lavas (samples 159 and 169). The silicate and carbonate fractions of the three Toro Ankole carbonatite lavas have been analysed separately, reporting suffix "S" to indicate the silicate fraction (carbonate component removed after HCl leaching), "C" to indicate the carbonate fraction (i.e., the HCl leached aliquot) and "WR" to indicate the whole-rock fraction (Table 5 and Appendix 1). The very young age of the volcanic activity in Toro Ankole and Virunga (Bufumbira) areas, coupled with the low Rb/Sr, Nd/Sm, U/Pb and Th/Pb ratios of the analysed samples, led to a radiogenic ingrowth. Consequently, no age corrections were applied to the measured Sr, Nd, Pb isotopic ratios reported in the Table 5 and in Fig. 9 and Fig. 10.

The $^{87}Sr/^{86}Sr$ isotopic ratios in Toro Ankole mildly ultrabasic lavas range from 0.70480 to 0.70563, higher than present-day Bulk Silicate Earth (BSE = 0.70445). This is observed for the ultramafic nodules too ($^{87}Sr/^{86}Sr$ = 0.70459–0.70499; Fig. 9a). Katwe-Kikorongo and Katunga mildly ultrabasic lavas show comparable Sr isotopic ratios, whereas the mildly ultrabasic lava 55 sample from Bunyaruguru is slightly more radiogenic. Bufumbira samples exhibit higher $^{87}Sr/^{86}Sr$ (0.70580–0.70708; Fig. 9a). The whole-rock $^{87}Sr/^{86}Sr$ ratios of the two carbonatite samples from Fort Portal (16WR and 17WR) are lower than BSE (0.70415 and 0.70405), whereas the Katwe-Kikorongo sample (79WR) falls within the range of the moderately ultrabasic rocks ($^{87}Sr/^{86}Sr$ = 0.70530). The carbonate fractions of these three rocks are characterized by lower $^{87}Sr/^{86}Sr$ ratio than the whole rock aliquots and silicate portions, with differences much higher than analytical errors. These differences indicate the absence of full isotopic equilibrium between the silicate and carbonate aliquots for the three carbonatitic rocks (Fig. 9b).

The $^{143}Nd/^{144}Nd$ isotopic ratios for Toro Ankole mildly ultrabasic and Bufumbira rocks are lower than the present-day Chondritic Uniform Reservoir (ChUR; 0.51264; Fig. 9a) and show a relatively narrow variation (0.512515 and 0.512575). Less radiogenic

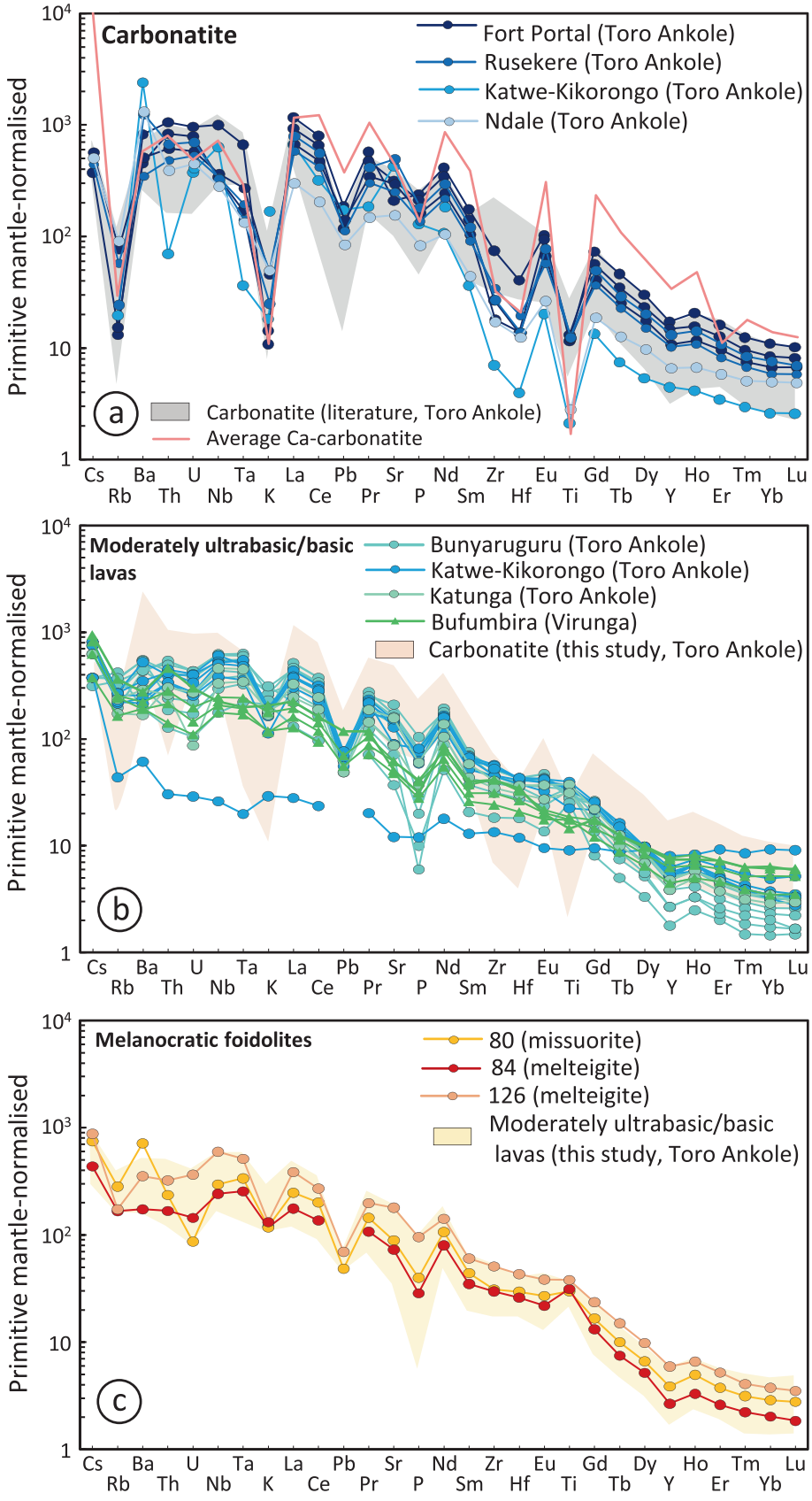

Fig. 7. Primitive mantle-normalised trace element pattern of the volcanic products from Toro Ankole and Virunga volcanic provinces. Primitive mantle composition is from Lyubetskaya and Korenaga (2007). (a) Strongly ultrabasic lavas and tuffs from Rusekere (34 and 35), Fort Portal (11, 16 and 17), Ndale (128), and Katwe-Kikorongo (79). Grey field: carbonatite compositions from literature. Pink line represents average calcium carbonatite (Woolley and Kempe, 1989; Chakhmouradian, 2006). (b) Moderately ultrabasic/basic lavas from Bunyaruguru (47, 49, 51, 53, 55, 57 and 58), Katwe-Kikorongo (81, 83, 85, 109, 110 and 114f) and Katunga (88 and 90), plus Bufumbira lavas (156, 159, 169 and 171). Light orange field: carbonatite samples from this study. (c) Melanocratic foidolites from Katwe-Kikorongo (80, 84 and 126). Light yellow field: moderately ultrabasic/basic lavas from Toro Ankole (this study). Colours and symbols as in Fig. 2a. (For interpretation of the references to colour in this figure legend, the reader is referred to the web version of this article.)

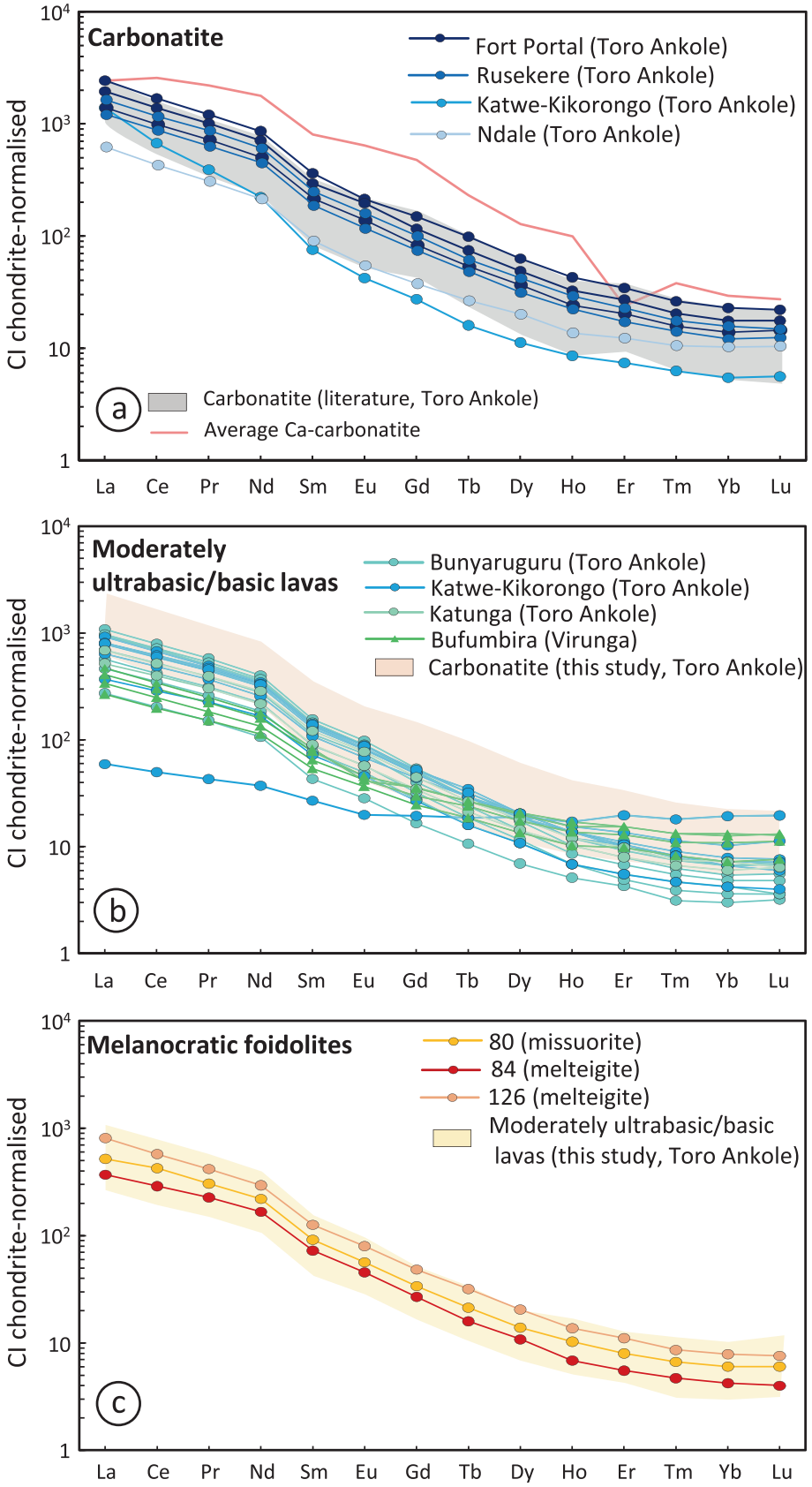

Fig. 8. Cl Chondrite-normalised REE patterns of volcanic products from Toro Ankole and Bufumbira provinces. Cl Chondrite composition is from King et al., 2020. (a) Strongly ultrabasic lavas and tuffs from Rusekere (34 and 35), Fort Portal (11, 16 and 17), Ndale (128), and Katwe-Kikorongo (79). Grey field: carbonatite compositions from literature. Pink line is average calcium carbonatite (Woolley and Kempe, 1989; Chakhmouradian, 2006). (b) Moderately ultrabasic/basic lavas from Bunyaruguru (47, 49, 51, 53, 55, 57 and 58), Katwe-Kikorongo (81, 83, 85, 109, 110 and 114f) and Katunga (88 and 90), plus Bufumbira lavas (156, 159, 169 and 171). Light orange field represents carbonatite values from this study. (c) Melanocratic foidolites from Katwe-Kikorongo (80, 84 and 126). Light yellow field: moderately ultrabasic/basic lavas 618 from Toro Ankole (this study). Colours and symbols as in Fig. 2a. (For interpretation of the references to colour in this figure legend, the reader is referred to the web version of this article.)

Table 4
Representative whole rock trace elements compositions of volcanic products from the WEAR, Virunga Volcanic Province (Bufumbira).

Sample	Locality	Rock Type	Rb	Sr	Ba	Cs	Sc	V	Cr	Co	Ni	Cu	Zn	Y	Zr	Nb	Hf	Ta
156	Bufumbira	Trachyandesite lava	166	803	1396	1.5	16	190	50	20		10	80	25	347	103	7.8	6
159	Bufumbira	Trachybasalt lava	116	976	1127	1.3	24	299	250	37		20	100	26	349	113	7.4	7.3
169	Bufumbira	Basanite Lava	75	752	975	0.6	28	295	1660	76	480	70	80	15	203	81	4.7	5.1
171	Bufumbira	Basanite Lava	111	973	965	1	26	291	1210	61	290	30	90	21	262	95	6	5.8

Sample	La	Ce	Pr	Nd	Sm	Eu	Gd	Tb	Dy	Ho	Er	Tm	Yb	Lu	Pb	Th	U	Ga
156	114	216	23.9	85.2	12.9	2.44	7.6	1	5.2	0.9	2.5	0.34	2.2	0.32	17	28.9	5.2	22
159	98.5	190	21.3	76.4	12.1	2.68	7.5	1	5.4	1	2.5	0.34	2.1	0.33	10	17.6	3.4	21
169	64.5	125	14.6	54.5	8.4	2.16	5.2	0.7	3.5	0.6	1.6	0.21	1.2	0.19		8.8	1.9	15
171	81.7	158	17.7	64.2	10.1	2.49	6.3	0.9	4.5	0.8	2.1	0.28	1.8	0.28	8	13.4	2.5	18

Table 5
Representative radiogenic ($^{87}Sr/^{86}Sr$, $^{143}Nd/^{144}Nd$, $^{206}Pb/^{204}Pb$, $^{207}Pb/^{20}4Pb$, $^{208}Pb/^{204}Pb$) and stable ($\delta^{11}B$) isotope compositions of volcanic products from the WEAR, Toro Ankole (N' Fort Portal, Bunyaruguru, K-K = Katwe-Kikorongo, Katunga) and Virunga (Bufumbira) volcanic provinces.

Sample	Locality	Rock Type	$^{87}Sr/^{86}Sr$	$^{143}Nd/^{144}Nd$	$^{206}Pb/^{204}Pb$	$^{207}Pb/^{204}Pb$	$^{208}Pb/^{204}Pb$	$\delta^{11}B$
16 WR	N' Fort Portal	Carbonatite lava	0.704184	0.512583	19.469	15.641	39.853	
16S	N' Fort Portal	Silicate fraction	0.704300	0.512600	19.920	15.999	40.713	
16C	N' Fort Portal	Carbonate fraction	0.703883	0.512658	19.456	15.640	39.854	
17 WR	N' Fort Portal	Carbonatite lava	0.704052	0.512595	19.435	15.641	39.848	
17S	N' Fort Portal	Silicate fraction	0.704216	0.512604	19.303	15.784	39.902	
17C	N' Fort Portal	Carbonate fraction	0.703851	0.512597	19.459	15.630	39.857	
55	Bunyaruguru	Kamafugite lava	0.705626	0.512531	19.395	15.724	39.976	−3.3
65	Bunyaruguru	Ultramafic nodule	0.704585	0.512487	19.986	15.670	40.318	−1.9
79 WR	K-K	Carbonatite lava	0.705304	0.512497	19.281	15.718	40.204	6.6
79S	K-K	Silicate fraction	0.705390	0.512543	19.294	15.390	39.410	
79C	K-K	Carbonate fraction	0.704848	0.512497	19.255	15.709	40.162	
85	K-K	Leucitite lava	0.704878	0.512571	19.190	15.674	40.138	−6.1
110	K-K	Lava	0.704797	0.512575	19.124	15.659	39.907	
86	K-K	Ultramafic nodule	0.704989	0.512554	19.269	15.646	39.869	−6.6
95	K-K	Ultramafic nodule	0.704887	0.512529	19.416	15.637	39.886	2.0
90	Katunga	Ol melilitite lava	0.704831	0.512515	19.630	15.701	40.237	−7.7
159	Bufumbira	Trachybasalt lava	0.707083	0.512353	19.415	15.781	40.815	−8.3
169	Bufumbira	Basanite lava	0.705805	0.512489	19.400	15.708	40.432	−4.4

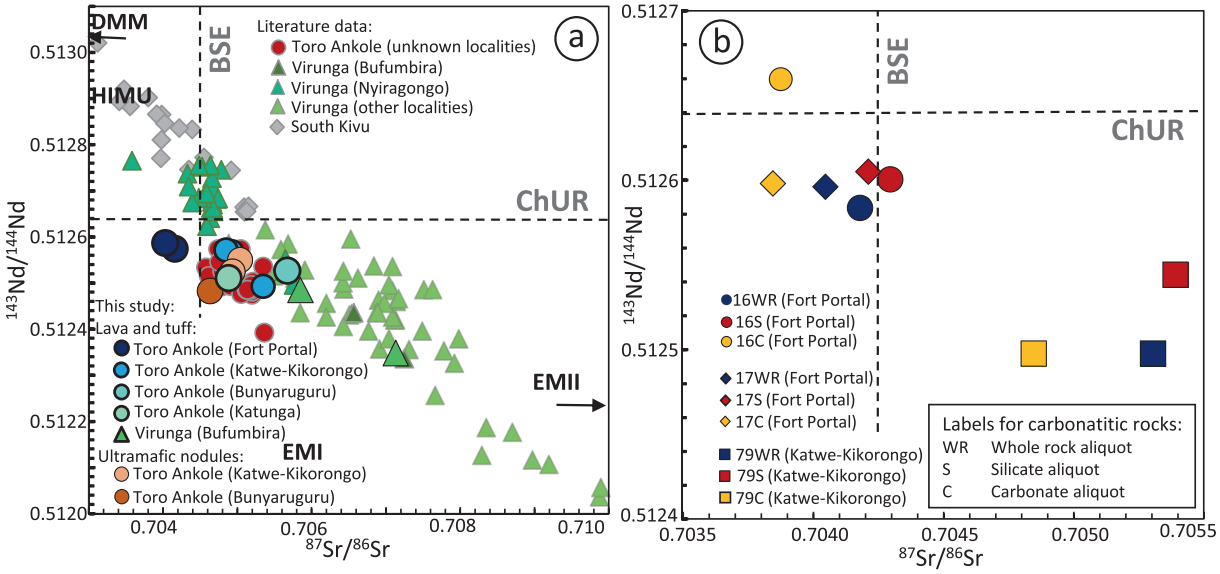

Fig. 9. (a) $^{143}Nd/^{144}Nd$ vs. $^{87}Sr/^{86}Sr$ diagram. Strongly ultrabasic lavas from Fort Portal (sample 16 and 17) and from Katwe-Kikorongo (sample 79); moderately ultrabasic/basic lavas from Bunyaruguru (sample 55), from Katwe-Kikorongo (sample 85 and 110) and Katunga (sample 90); Bufumbira lavas (sample 159 and 169) and ultramafic nodules from Bunyaruguru (sample 65) and Katwe-Kikorongo (sample 86 and 95) are plotted. Literature data as in Fig. 5. (b) $^{143}Nd/^{144}Nd$-$^{87}Sr/^{86}Sr$ diagram for strongly ultrabasic samples (16, 17 and 79). Dark blue symbols: whole-rock compositions, red symbols silicate fractions, dark yellow symbols: carbonate fractions. (For interpretation of the references to colour in this figure legend, the reader is referred to the web version of this article.)

$^{143}Nd/^{144}Nd$, ranging from 0.512487 and 0.512554, characterise the ultramafic nodules. The three aliquots analysed for the carbonatite samples (whole-rock, silicate and carbonate parts) show irregular differences, with the carbonate component being either more radiogenic (sample 16C), less radiogenic (sample 79C) or overlapping the silicate aliquot (sample 17C; Fig. 9b).

The $^{206}Pb/^{204}Pb$ isotopic ratios are much more variable than Sr-Nd isotopes (Fig. 10a). $^{206}Pb/^{204}Pb$ varies between 19.12, in Katwe-Kikorongo mildly ultrabasic lava 85, and 19.99 in an ultramafic nodule from Bunyaruguru (sample 65). The carbonate and silicate fractions, plus the whole rock composition of the carbonatite rocks do not show systematic variations. Fort Portal sample 16C shows $^{206}Pb/^{204}Pb$ (19.46) overlapping that of the whole-rock aliquot (sample 16WR; 19.46), but much lower than the silicate fraction (sample 16S; 19.92; Fig. 10b). The other sample from Fort Portal has a carbonate fraction (sample 17C; $^{206}Pb/^{204}Pb$ 19.46) very similar to that of whole-rock (sample 17WR; 19.44), but higher than the silicate fraction (sample 17S; 19.30). The Katwe-Kikorongo carbonate fraction (sample 79C) has $^{206}Pb/^{204}Pb$ slightly lower (19.26) than the whole-rock (sample 79WR; 19.28) and the silicate fraction (sample 79S; 19.29), but generally within analytical error (Fig. 10b). The $^{207}Pb/^{204}Pb$ is less variable, ranging between 15.67 and 15.72 in Toro Ankole mildly ultrabasic samples, with Bufumbira having higher values, 15.71–15.78 (Fig. 10c). All samples plot above the Northern Hemisphere Reference Line (Hart, 1984) showing higher $^{207}Pb/^{204}Pb$ and right of the Geochron (Fig. 10c). Ultramafic nodules, together with Fort Portal carbonatites, show the lowest values (15.64–15.67 and 15.64, respectively), whereas Katwe-Kikorongo carbonatite reaches a higher value of 15.72 (Fig. 10c). Moreover, the silicate fraction (15.78–16.00) from Fort Portal has higher $^{207}Pb/^{204}Pb$ than the carbonate aliquot (15.63–15.64), in contrast to Katwe-Kikorongo (79S = 15.39 and 79C = 15.71). $^{208}Pb/^{204}Pb$ isotopic ratios are more homogeneous in all the Toro Ankole samples, varying between 39.85 and 40.32. Bufumbira values are slightly higher (up to 40.82).

Whole-rock $\delta^{11}B$ values mostly fall within the common mantle values typical of MORB and OIB (from −3 to −9 ‰; Agostini et al., 2021 and references therein), albeit with significant variations, covering the entire mantle range, with values as light as −8.3 ‰ for Bufumbira sample 159 to quite heavy (−3.3 ‰; mildly ultrabasic lava sample 55 from Bunyaruguru; Fig. 11a). However, the two ultramafic nodules (sample 95 from Katwe-Kikorongo and sample

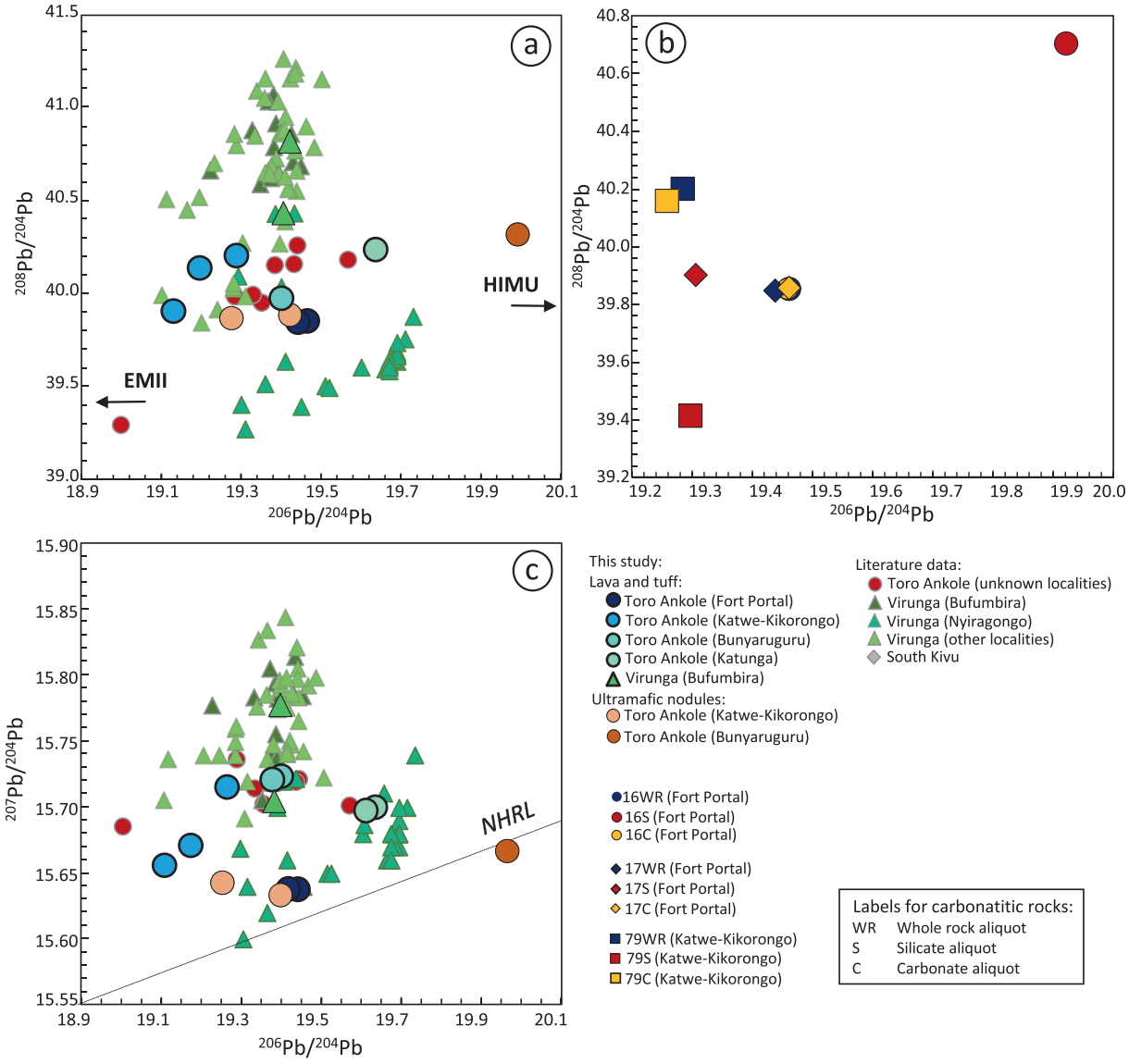

Fig. 10. (a) $^{208}Pb/^{204}Pb$ vs. $^{206}Pb/^{204}Pb$ diagram. (b) $^{208}Pb/^{204}Pb$ vs. $^{206}Pb/^{204}Pb$ diagram for strongly ultrabasic samples (16, 17 and 79). (c) $^{278}Pb/^{204}Pb$ vs. $^{206}Pb/^{204}Pb$ diagram. NHRL: North Hemisphere Reference Line (Hart, 1984).

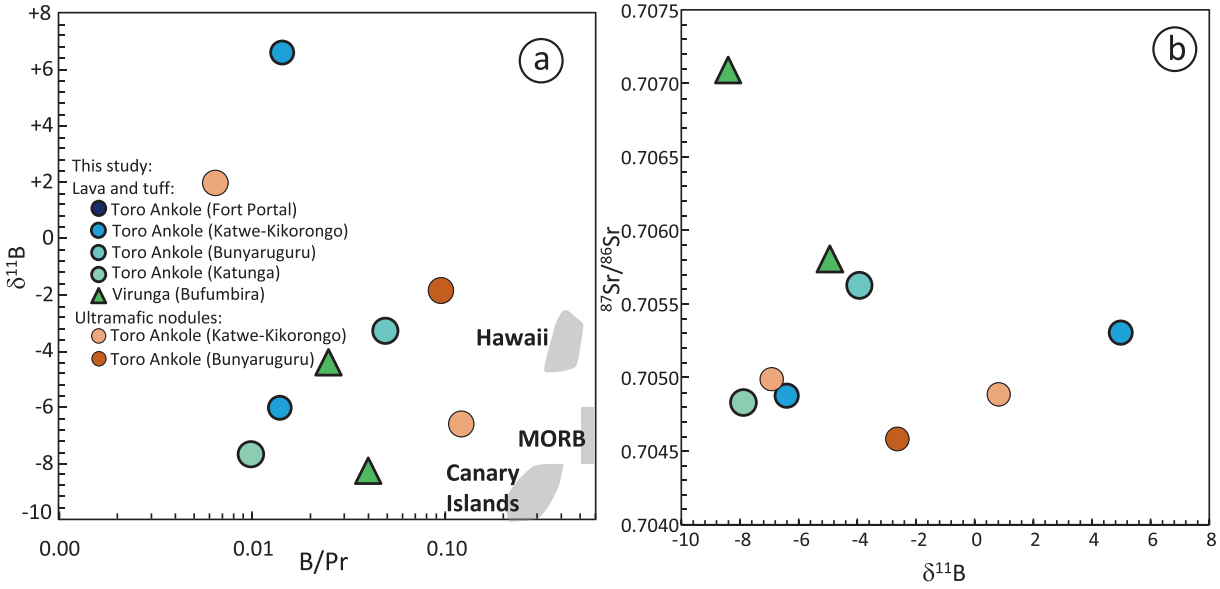

Fig. 11. (a): $\delta^{11}B$ vs. vs. B/Pr diagram. (b) $^{87}Sr/^{86}Sr$- $\delta^{11}B$ diagram. Samples are carbonatite from Katwe-Kikorongo (sample 79), lava from Bunyaruguru (sample 55), from Katwe-Kikorongo (sample 85), Katunga (sample 90) and Bufumbira (sample 159 and 169) and ultramafic nodules from Bunyaruguru (sample 65) and Katwe-Kikorongo (sample 86 and 95). Values for mantle end-members from Agostini et al., 2021 and references therein.

65 from Bunyaruguru), and the carbonatite sample 79 cluster around $\delta^{11}B$ of 0 ± 2 ‰, +6.6 ‰, respectively (Fig. 11a). Rough positive $^{87}Sr/^{86}Sr$ vs. $\delta^{11}B$ and negative $^{143}Nd/^{144}Nd$ vs. $\delta^{11}B$ correlation (Fig. 11b and Electronic Appendix 5) are observed for Toro Ankole samples, where samples with $\delta^{11}B > -5$ ‰ usually have $^{87}Sr/^{86}Sr > 0.7049$, well above the BSE value. In contrast, samples from Virunga follow a negative Sr-B isotope trend.

4. Discussion

4.1. Petrographic and mineral chemical implications of the carbonatites

The presence of carbonate-rich volcanic breccias is a very common aspect, but its origin remains controversial (e.g., see discussion in Innocenzi et al., 2021). Despite primary carbonates are observed as phenocrysts and in the ash-size matrix in Toro Ankole rocks (e.g., Eby et al., 2009), Barker (2007) proposed a secondary origin for the carbonates cementing the lapilli in some Fort Portal rocks, ascribing them to precipitation from carbonate-saturated meteoric waters.

The carbonate fraction in the tuffs analysed in this study shares similar features in the various volcanic districts of Toro Ankole albeit it occurs in variable texture. In many cases (e.g., sample 70 from Bunyaruguru and sample 91 from Katwe-Kikorongo), carbonates define a microcrystalline to sparry and drusy texture (Fig. 3a–b; Figs. EA3 a–d in Electronic Appendix 2), but they also occur as crystalline rims around lapilli, suggesting several phases of dissolution and precipitation (Figs. EA1 a–b in Electronic Appendix 2). The carbonate rims coating the lapilli and the meniscus cements show -variable and inhomogeneous thickness around the clasts (EA3 c–d in Electronic Appendix 2) suggesting a growth under the action of gravitational force, probably representing the first diagenetic products. Moreover, as these cements do not show a consistent orientation and are often associated with ghosts of previous unstable crystals, they could be related to different rapid dissolution and reprecipitation stages. Dogtooth-shaped calcite, on the other hand, is the final cement that fills almost all the cavities. It consists of large crystals with straight edges probably due to slow growth. All these fabrics usually indicate conditions of development in a vadose or phreatic zone (Flügel, 2004). Leaching of carbonates and CaO-rich products would have led to meteoric and percolation water enriched in calcium carbonate. The hot and humid weather of the area would have facilitated not only leaching and the mobilization of Ca^{2+} ions needed for the formation of $CaCO_3$, but also the precipitation of calcite as secondary cement. Also the slightly MgO-enriched and BaO- and SrO-poor compositions recorded by SEM-EDS and EMP analyses (Fig. 3a–b) in the sparry calcite cement are compatible with a vadose environment (Brand and Veizer, 1980).In terms of CaO-MgO-FeO classification, the carbonatite lavas and tuffs analysed in this study fall in two fields: calcium carbonatite for the Katwe-Kikorongo lava and ferrocarbonatite for lavas and tuffs from the Fort Portal, Ndale and Rusekere fields (Fe_2O_{3tot} = 5.61–13.68 wt% and CaO = 25.17–30.25 wt%). This geographic difference is, however, related more to the composition of the silicate phases than to the chemical composition of the carbonate fraction itself (see discussion in Mitchell and Gittins, 2022). Samples with high Fe_2O_{3tot} also show higher SiO_2 content (up to 21.8 wt%) reflecting the higher modal contents of clinopyroxene, phlogopite and magnetite. On the other hand, the EMP analyses indicate an almost pure calcium carbonate composition for Fort Portal lava sample 17, with 0.12–4.71 wt% FeO_{tot}.

4.1.1. Carbonatite-silicate magma relationships

The association of carbonatites and ultrabasic silicate lithologies, such as those found in Toro Ankole volcanic province, is relatively common: ~80 % of worldwide carbonatites are associated with silicate igneous rocks with variable alkali contents and SiO_2 commonly in the ~35–60 wt% range, mainly nephelinites, melilitites, phonolites and their plutonic equivalents (Woolley and Kjarsgaard, 2008). Fort Portal carbonatites have been interpreted as the result of immiscibility from a parental olivine-melilitite magma at a pressure of ~1 GPa, which underwent olivine fractionation before entering the miscibility gap (Eby et al. 2009). The Fort Portal carbonatite tuffs reported here contain carbonatite lapilli (e.g., Fig. EA1 a–d Electronic Appendixes 2; data from Electronic Appendix 3 and 4). A detailed petrographic study and mineral chemical analyses highlighted the absence of any silicate volcanic clasts.

Interestingly, Zartner (2010) in a comprehensive study on the lapilli tuffs from Toro Ankole, highlighted a progressive change in

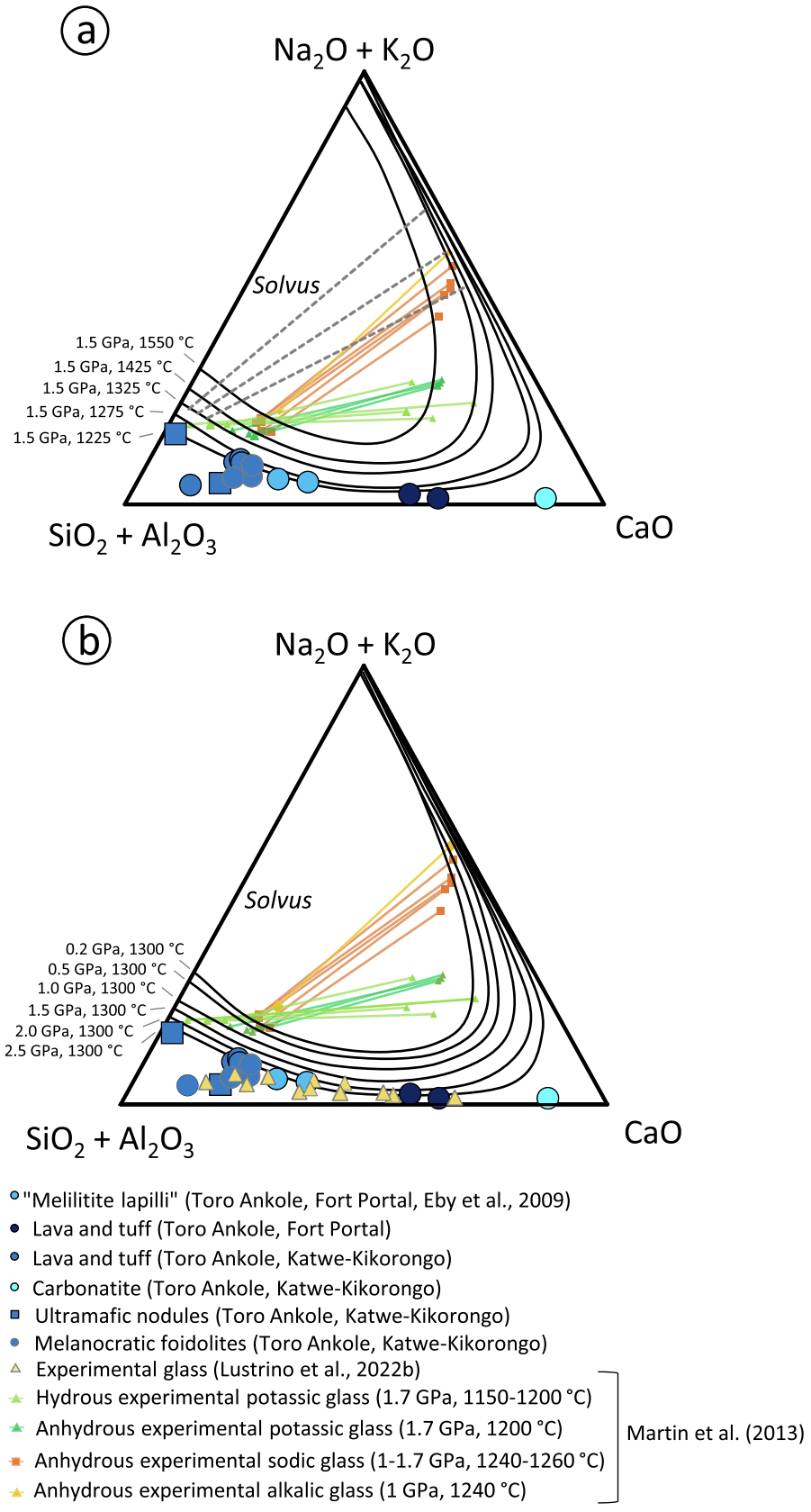

Fig. 12. $Na_2O + K_2O$-($SiO_2 + Al_2O_3$)-CaO diagrams showing solvus gap between silicate and carbonatite liquids, experimentally determined by Brooker and Kjarsgaard (2011). (a): solvus lines for isobaric conditions (P = 1.5 GPa; CO_2-saturated) with T ranging between 1125 and 1550 °C. (b): solvus lines for isothermal conditions (T = 1300 °C; CO_2-saturated) at P ranging between 0.2 and 2.5 GPa. Experimental results on liquid immiscibility from Martin et al. (2013) are also plotted for Na_2O-rich starting materials, K_2O-rich starting material (potassic), and starting materials with the same amount of Na_2O and K_2O (alkalic). Experiments were conducted at 1220–1260 °C and 1–1.7 GPa, for the CO_2 bearing terms; and 1150–1200 °C and 1.7 GPa for the CO_2 and H_2O bearing compositions (light green). Experimental glass data from Lustrino et al. (2022b) are reported for comparison. (For interpretation of the references to colour in this figure legend, the reader is referred to the web version of this article.)

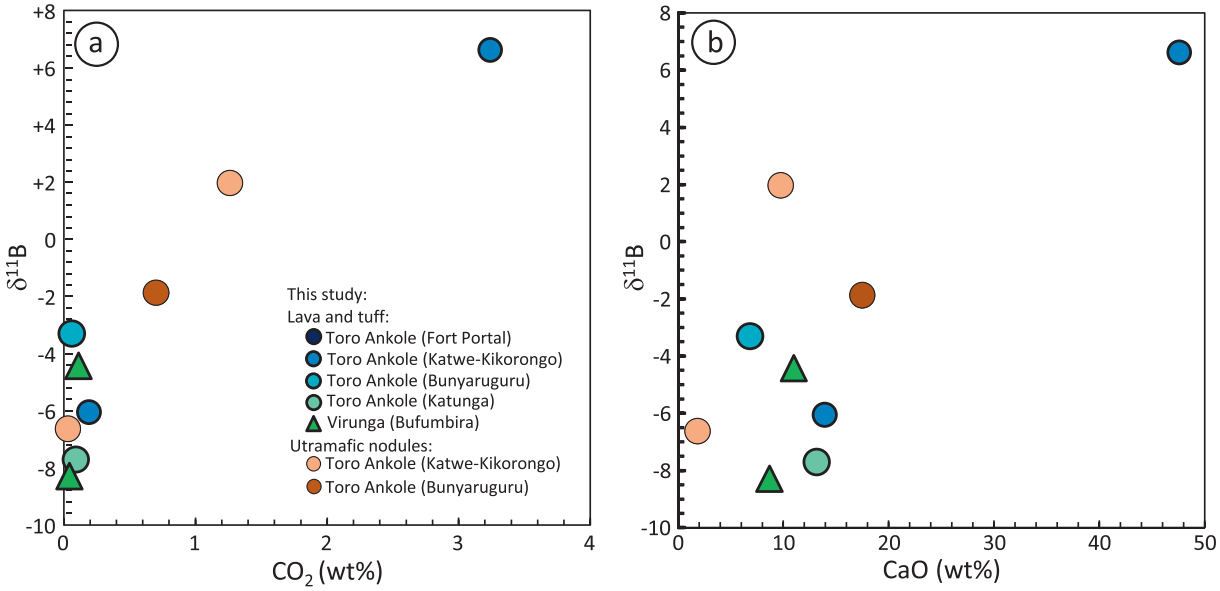

Fig. 13. (a) $\delta^{11}B$ vs. CO_2 diagram. (b) $\delta^{11}B$ vs. CaO diagram. Carbonatite from Katwe-Kikorongo (sample 79), lava from Bunyaruguru (sample 55), from Katwe-Kikorongo (sample 85), Katunga (sample 90) and Bufumbira (sample 159 and 169) and ultramafic nodules from Bunyaruguru (sample 65) and Katwe-Kikorongo (sample 86 and 95) are plotted.

composition among the volcanic districts, from carbonatite to kamafugite tuffs in a southward direction. Fort Portal, Rusekere and Ndale tuffs are characterized by a carbonate matrix and lapilli groundmass with CaO >30 wt% and SiO_2 < 15 wt%, whereas lapilli from Bunyaruguru, Katwe-Kikorongo and Katunga contain olivine, calcite, clinopyroxene, melilite, kalsilite and perovskite, which are reflected in the major oxide compositions (SiO_2 = 33–45 and K_2O + Na_2O up to 14 %). Our observations fit well with the pattern described by Zartner (2010).

Experimental studies at low pressure (0.1 to 1 GPa) and relatively high temperature (~1000 °C) and melt inclusions data (e.g., Guzmics et al., 2015) indicate that carbonatitic magmas may separate immiscibly from melilitite-nephelinite melts. The process would produce melts enriched in CaO (~32–41 wt%) and in LREE, Sr and Ba (Yaxley et al., 2022). Other studies (e.g., Schmidt and Weidendorfer, 2018) indicate that immiscibility between silicate and carbonatite melts can be achieved only if the starting melt composition is ultrabasic and alkali rich. This finding was recently confirmed by the experimental study of Lustrino et al. (2022b), who found no trace of silicate-carbonate melt immiscibility process in $CaCO_3$-doped ultrabasic compositions with low total alkali contents (1.67–4.57 wt%) at low pressures (0.2 GPa) in the 1000–1300 °C range. Contrary to this latter evidence, the two-liquid field seems to expand also in alkali-free compositions, at 2–3 GPa (Novella et al., 2014). What emerges is that this topic remains poorly constrained, despite decades of petrological studies, especially concerning the role of alkalis and the K_2O/ Na_2O ratio in determining the existence and width of the miscibility gap between silicate and carbonate liquids.

The compositions of Fort Portal and Katwe-Kikorongo carbonatites and moderately ultrabasic rock samples are plotted in Fig. 12, where they are compared to ultrabasic samples from Eby et al. (2009) to locate the possible silicate end-member at Fort Portal. The diagrams show the experimentally determined solvus between silicate and carbonatite liquids (Brooker and Kjarsgaard, 2011), at pressures ranging between 0.2 and 2.5 GPa and 1125–1550 °C. To better define the effect of K_2O on liquid immiscibility, experimental results from Martin et al. (2013) have been plotted too. Light and dark green lines represent tie lines connecting K_2O-rich silicate and carbonate liquid compositions in hydrous and anhydrous conditions, respectively P = 1.7 GPa and T = 115 0–1200 °C; Martin et al., 2013). The coexisting immiscible liquids reported by Martin et al. (2013) partially fall on the solvi obtained by Brooker and Kjarsgaard (2011) for Na_2O-rich systems (Fig. 12a–b). For Fort Portal compositions, both carbonatite and moderately ultrabasic samples fall close to the immiscibility gap lines at 2.5 GPa (Brooker and Kjarsgaard, 2011). The lack of more experimental data at higher pressure makes hard to predict if they would have crossed the solvus at greater depths. The same is observed for the Katwe-Kikorongo samples. Considering the low alkali content of the analysed rocks, the parental silicate melt would have been originated at pressures > 2.5 GPa, to enter the immiscibility gap, which corresponds to depths higher than that proposed by Eby et al. (2009).

The Sr, Nd and Pb isotopic differences among the north and south Toro Ankole volcanic districts can contribute to cast light on the reciprocal relationships. Fort Portal carbonatite lavas have depleted Sr-Nd isotopic ratios (Fig. 9a–b), coupled with radiogenic $^{206}Pb/^{204}Pb$ (Fig. 10a–d), indicating the influence of a HIMU end-member. The Katwe-Kikorongo carbonatite lava seems to be derived from a more Sr-Nd isotopically enriched mantle sources and slightly less radiogenic $^{206}Pb/^{204}Pb$. In the three carbonatite samples investigated here, the isotopic data for the silicate and carbonate fractions of these carbonatite lavas differ, suggesting isotopic disequilibrium between the silicate and carbonate components. Assuming that this is not related to the alteration of the carbonate fraction, the bias between the isotopic compositions of the two aliquots can be considered as a further indication of local differences in mantle source lithologies. The sampling of adjacent metasomatic veins would explain the coexistence of silicate and carbonate portions with different isotopic ratios.

Isotopic differences between the separated carbonate and silicate fractions of the carbonatite lavas suggest disequilibrium between the two components (Figs. 9b and 10b), which disagrees with the conclusions of Eby et al. (2009) that the carbonatite originated by immiscibility. The carbonate fraction always shows $^{87}Sr/^{86}Sr$ (0.70385–0.70485) lower than the silicate aliquot (0.70422–0.70539; Fig. 9b).

The higher Sr isotopic ratio of the silicate vein where most of Rb would be stored, could be also considered a clue of the young age of such veins found in the mantle source. Even with the strong enrichment in Sr of one of the aliquots, and a consequently low Rb/Sr ratios in the carbonatites, the young age of emplacement (<0.2 Ma) does not leave time for any detectable radiogenic ^{87}Sr ingrowth. Given the smaller variation of Sm/Nd ratios the age-shift of Nd isotopes is wholly negligible. This clear lack of equilibrium between the silicate and carbonate fractions of the carbonatites may indicate a heterogeneous and veined mantle source beneath Toro Ankole, as the carbonatitic magma would have sampled a neighbouring and slightly different silicate portion. The presence of more than one component in the mantle source of Toro Ankole magmatism has been already highlighted by Rosenthal et al. (2009): based on isotopic data, they proposed the presence of an older MARID-type assemblage, which would have been coupled with carbonate and phlogopite veins, younger than 100 Ma. They suggested heterogeneous Sr ratios in the veins, depending on the abundance of carbonate, phlogopite and apatite, but also on the phlogopite age in the MARID suites.

The Sr isotope differences are not mirrored by $^{143}Nd/^{144}Nd$ and Pb isotopic ratios, for which no systematic variation can be observed among the silicate and carbonate components. However, the Pb isotopic ratios of the carbonate fraction are very close to the whole rock values, pointing out that the main lead sources of the magma are carbonate-bearing phases in the mantle.

Literature data for $\delta^{11}B$ in carbonate-rich igneous samples ranges from −8.6 to +5.5 ‰ (Hulett et al., 2016), whereas common mantle-derived basaltic rocks (either MORB or OIB) cluster in a much narrower interval, $\delta^{11}B$, mostly between −9 and −3 ‰; (Section 3.4). The B isotopic ratio of carbonatite sample 79 shows highly positive values (+6.6 ‰), and two other samples of our dataset (ultramafic nodules 95 and 65) have higher $\delta^{11}B$ values than common mantle. In a $\delta^{11}B$ vs. CO_2 as well as $\delta^{11}B$ vs. CaO content plots (Fig. 13a and 13b), it is evident that ^{11}B-enrichments are paralleled by increases in C and the CaO contents. This may indicate the occurrence of an Altered Oceanic Crust (AOC), component, possibly coupled with sedimentary limestones, recycled in the mantle beneath the WEAR, which is responsible for the supply of both C and heavy B. AOC is often serpentinised and contains calcite veins, evolving into ophicarbonates with $\delta^{11}B$ up to 41 ‰ during subduction (Marschall, 2018).

4.2. Mineralogical and petrographic constraints on kalsilite-bearing and kalsilite-free lavas

The presence of kalsilite in most of the samples denotes the coupled K_2O-rich and SiO_2-poor magma composition, as also testified by the compositions of clinopyroxenes. In kalsilite-bearing lavas, clinopyroxene phenocrysts are occasionally surrounded by a reaction corona of euhedral laths of totally altered melilite or anhedral patches anomalously rich in CaO (CaO = 60.37–61.16 wt %, MgO = 0.34–0.56 wt% and FeO = 0.08 wt%). Ca-rich reaction rims around corroded and partially resorbed clinopyroxenes have been also found in the kamafugite lapilli tuff (sample 70; Figs. EA3 e–f Electronic Appendix 2). This petrographic evidence highlights a late instability of clinopyroxene in the kamafugitic magma as consequence of changes in magma chemistry not much before eruption. The crystallization of melilite and carbonate at the expense of clinopyroxene clearly indicates an increase of CaO activity and decrease of SiO_2 in the system. A similar abrupt change has been recorded in other ultrabasic systems where the presence of monticellite rims around forsteritic olivine (e.g., Lustrino et al., 2019b) and melilite reaction rims around clinopyroxene (Lustrino et al., 2022a) have been interpreted as due to the assimilation of sedimentary carbonates. In the Ugandan samples, the instability of clinopyroxene rims associated with increased stability of melilite and carbonates could be associated with the presence of bicarbonate-rich fluids, probably released by the carbonate-rich veins. What emerges is that these features are not incompatible with the ultimate primitive origin of Ca-enrichment of the investigated rocks. The presence of two different processes (i.e., primary ultrabasic compositions, that experienced secondary Ca-enrichment) is demonstrated to occur naturally (e.g., Gozzi et al., 2014; Lustrino et al., 2019b).

Not all the moderately ultrabasic samples from Toro Ankole host kalsilite: actually, olivine melilitites occur at Katunga (Fig. 3c–d) and leucitites and nephelinite at Katwe-Kikorongo (Figs. EA6 a–d Electronic Appendixes 2). Olivine melilitites lack clinopyroxene and are rich in foids, phlogopite and melilite. Leucitites and nephelinite mainly differ by the nature of the main feldspathoids, as leucite is found in both rock types, whereas nepheline, abundant in the groundmass, replaces kalsilite. Mineral compositions are comparable for all phases from the kamafugites, olivine melilitites, leucitites and nephelinites. As in kamafugite, leucitite clinopyroxene needs Al and Fe^{3+} to fill the T site due to the extremely low silica of the magma. The similar petrographic, mineral chemical and geochemical features may point to a close relationship between kalsilite-bearing and kalsilite-free rocks of Toro Ankole.

Geochemical compositions are also uniform, especially as regards major oxide contents. Kamafugites are ultrabasic, TiO_2- and CaO-rich rocks. The alkali budget differs slightly, with slightly lower K_2O and higher Na_2O in the leucitite, nephelinite and olivine melilitites than in the kamafugites. Nevertheless, they are all potassic, two samples reaching ultrapotassic composition. Harker diagrams for trace elements (Electronic Appendix 5) show considerable overlap between kamafugite and the kalsilite-free rocks, with comparably high enrichment. They display similar patterns on mantle- and the CI-chondrite normalised diagrams (Figs. 7 and 8), but with less pronounced troughs at P and with slightly lower LREE/HREE fractionation than the kalsilite-bearing rocks from Bunyaruguru.

All the variations observed in the geochemical, isotopic, petrographic and mineral chemical data among the moderately ultrabasic lavas from the different volcanic districts of Toro Ankole are small, suggesting that all these rocks may have been produced by partial melting of a similar, heterogeneous mantle source with some differences in the mineral assemblage. Olivine melilitites from Katunga and leucitites and nephelinites from Katwe-Kikorongo show slightly higher CaO contents than the Bunyaruguru kamafugite, probably due to presence of more clinopyroxene and carbonate in the metasomatic veins. Katwe-Kikorongo and Katunga also show lower K_2O content and a slightly higher Na_2O budget which would explain by a source with higher clinopyroxene/phlogopite than Bunyaruguru. TiO_2 content is also slightly higher, probably caused by higher amounts of Ti-rich phases in the source. For these reasons, the whole moderately ultrabasic rock group (e.g., kalsilite-free and kalsilite-bearing products) will be discussed together hereafter.

Many experimental studies have been carried out on kamafugite rocks (e.g., Lloyd, 1985; Arima and Edgar, 1983; Edgar and Vukadinovic, 1992). Lloyd (1985) demonstrated that the main differences between the products of Toro Ankole (olivine melilitite, leucite clinopyroxenite and leucite-kalsilite clinopyroxenite) may be related to alkali loss during the early phases of magmatic activity. A process involving alkali loss is also envisaged by Eby et al. (2009) to explain the presence of alkali-poor melilititic lapilli within the Toro Ankole blanket tuff formation. The slightly higher Na content in Katunga samples would cause melilite crystallization, leading to a different parageneses among the lavas from Katunga, Katwe-Kikorongo and Bunyaruguru, which need not be

related to dissimilar depths or fractional crystallization (Lloyd, 1985). However, alkali loss would not explain our new data, as Katunga and Katwe-Kikorongo samples show not only a lower potash content, but also higher Na_2O.

4.3. Mantle source constrains of Toro Ankole silicate rocks

The occasional presence of crustal xenoliths affects the whole-rock compositions of the tuffs (Barker and Nixon, 1989; Eby et al., 2009). Also the lavas may contain accidental fragments, but accurate hand-picking under binocular microscope removed most extraneous materials before powdering for chemical analysis. For the lavas, however, the presence of accumulated phenocrysts may have influenced the analysed composition too.

The exotic compositions of ultrabasic samples are characterized by variable alkali enrichment (Na_2O + K_2O = 4.05–8.32 wt%; Fig. 2a). Lava sample 110 is pervasively altered and will not be further considered in the discussion. The inferred magma composition was volatile-rich, as inferred by the high CO_2 and LOI content. which is also testified by the explosive character of most of eruptions.

The negative anomalies at K and P in primitive mantle-normalised diagrams (Electronic Appendix 5) might suggest, at a first sight, the presence of residual K- and P-rich phases (phlogopite and apatite) in the mantle source (Fig. 7b). This, however, would be at odds with the overall K-rich composition of the moderately ultrabasic products and with their moderate content of P_2O_5 (up to 1.57 wt%). Instead, it could be seen as a buffering effect, caused by the less extreme partition coefficients of K and P, or as the result of a source highly enriched in neighbouring incompatible elements and high incompatible elements (e.g., Sr = 1129–3307 p pm, ΣREE = 473–1064 ppm; Fig. 8b).

The flat to poorly fractionated MREE/HREE pattern does not match with the presence of residual garnet in the source, which would have produced much more fractionated MREE/HREE trends (Fig. 7b). Garnet has been found only in one of the many ultramafic nodules from Fort Portal (a garnet-lherzolite from Kalyango cone; Barker and Nixon, 1989) which could indicate the derivation of most melts from relatively shallow mantle depths, corresponding to the lithospheric mantle ~80–90 km thick under the investigated area (Fig. 1a; Afonso et al., 2022).

Isotopic constraints highlight the involvement of a heterogeneous mantle source, in agreement with earlier works (e.g., Bell and Powell 1969; Rosenthal et al., 2009; Muravyeva et al., 2014). Radiogenic $^{87}Sr/^{86}Sr$ (0.70479–0.70563) and $^{206}Pb/^{204}Pb$ (19.12–19.63) ratios of the Toro Ankole mildly ultrabasic lavas, together with unradiogenic $^{143}Nd/^{144}Nd$ (0.512515–0.512575) ratios plot between the HIMU (High-μ) and EMI-EMII end-members, outlining an isotopically enriched mantle source (Figs. 9a and 10a–c).

Significant crustal contamination and assimilation of upper crustal lithologies (granitoid to gneissic) during magma ascent to the surface is unlikely, considering the almost constant $^{87}Sr/^{86}Sr$ with increasing SiO_2. Limited assimilation of SiO_2-rich basement rocks would lead to the crystallization of leucite rather than kalsilite and clinopyroxene rather than melilite (Holmes, 1950).

Boron can track the presence of recycled materials in mantle sources, as it is very sensitive to the addition of subducted crustal lithologies (e.g., Agostini et al., 2021). Recycled materials can strongly modify the $\delta^{11}B$ of the mantle, spanning the range from −20 to + 40 ‰ in different environments, with negative values related to continental crustal lithologies (Chaussidon and Albarède, 1992), and positive values usually related to interaction with marine sediments and seawater-altered rocks (e.g., Agostini et al., 2021). The $\delta^{11}B$ values for the Toro Ankole rocks support the occurrence of a heterogeneous mantle source, in which subducted crustal materials played a key role. Samples with lower $^{87}Sr/^{86}Sr$, higher $^{143}Nd/^{144}Nd$ and low $\delta^{11}B$, which fall within the mantle ranges defined by MORB (−8 to-6 ‰), have $\delta^{11}B$ more akin to common mantle, whereas samples with higher $\delta^{11}B$ and $^{87}Sr/^{86}Sr$ (Fig. 11b) retain evidence of the recycled ^{11}B enriched material, such as AOC and/or marine limestones (Fig. 13a–b). The involvement of AOC-like or limestone-bearing metasomatic component in the mantle source of Toro Ankole lavas is confirmed by the positive CO_2-$\delta^{11}B$ and CaO-$\delta^{11}B$ correlation of samples showing C- and CaO-enrichments (Fig. 13a–b).

The subducted AOC and marine carbonates inputs is often associated with the occurrences of amphibole and phlogopite veins in the mantle beneath collisional areas (e.g., Kelemen and Manning, 2015). This refertilization of the mantle underlying the WEAR has been related to different events: an older stage for the clinopyroxene- and phlogopite-rich assemblage, and a younger one (<100 Ma) for carbonate-bearing assemblages (Rosenthal et al., 2009). This is consistent with the new data (e.g., $\delta^{11}B$) reported in this study, as old AOC probably would have a $\delta^{11}B$ very similar to the mantle range (Marschall, 2018).

4.4. Influence of the mantle structure on Toro Ankole magmatism

The WEAR volcanic centres insist on a rheologically weak Proterozoic suture zone bordering the western margin of the Tanzanian Craton (De Waele et al., 2008; Fig. 1). According to this view, the cratonic lithosphere focuses decompression adiabatic melting and edge-driven convection (e.g., King and Anderson, 1998). An alternative to this view considers the Toro Ankole region to be part of continuous cratonic lithosphere connecting the Congo and Tanzanian blocks (Rosenthal et al., 2009; Link et al., 2010). However, a recent thermochemical model for the whole central-southern Africa confirms the existence of two separate cratons (Afonso et al., 2022).

The source of Toro Ankole magmas is considered to be volatile-rich, explaining the high carbonate content and the high volume of pyroclastic deposits compared to lavas. Furthermore, the abundance of carbonatites and ultrabasic silicate compositions (e.g., melilitites, kamafugites, leucitites) are compatible with hydrous, phlogopite-bearing carbonated mantle (e.g., Rosenthal et al., 2009; Foley et al., 2012). The most common hydrous phases at realistic geotherms in the upper mantle are pargasitic amphibole up to ~3 GPa, followed by phlogopite, which is stable in a peridotite matrix up to ~6–8 GPa or 9–12 GPa, depending on the mineral assemblage (Foley and Pintér, 2018).

The strong thickness gradient, with lithosphere-asthenosphere boundary thinning from ~160 km beneath the Tanzanian Craton to ~80–90 km beneath the WEAR, evidenced by recent thermochemical and tomographic models (Afonso et al., 2022), could focus melting towards the shallowest LAB (lithosphere-asthenosphere boundary) portions identified in the WEAR and the eastern branch of EAR. To explain the high K_2O budget (up to 7.05 wt%) of Toro Ankole samples, high abundances of phlogopite, rather than amphibole, are required. The WEAR lithospheric keel should have experienced low-degree partial melting as consequence of the heat released by passively upwelling sub-lithospheric mantle, thermally insulated beneath the thick Tanzanian cratonic lithosphere. The presence of phlogopite as well as carbonates depresses the solidus temperature, allowing partial melting without requiring a thermal anomaly in the form of a strong, deep-rooted mantle plume. We suggest that the carbonate stored in the mantle beneath Toro Ankole is derived from older subducted material, probably represented by ophicarbonates and recycled marine carbonates, as highlighted by isotopic data.

The ultimate phlogopite-carbonate-rich mantle assemblages are likely the consequence of repeated metasomatic fertilization and oxidation events that occurred during the various phases of

accretion of the African continent. Metasomatic veins would have been produced by very mobile magmas during low-degree partial melting of a K-rich and incompatible element-rich source (e.g., Foley, 1992). For the WEAR, Rosenthal et al. (2009) suggested two metasomatic events resulting in a MARID-type (mica, amphibole, rutile, ilmenite and diopside) assemblage, followed by a carbonate-rich veins network.

Recent works allows us to suggest the importance of other mineral phases in the paragenesis of kamafugites. The involvement of uncommon phases in the mantle, such as phlogopite, clinopyroxene, apatite, possibly perovskite and titanite, for kamafugite magmas is supported by isotopic (e.g., high $^{87}Sr/^{86}Sr$), as well as major oxide and trace element constraints. Moreover, the presence of these phases beneath the WEAR is testified by the ultramafic clinopyroxenite to glimmerite nodules (e.g., Lloyd, 1981; Link et al., 2008; Pitcavage et al., 2021). Therefore, we hypothesize a non-lherzolitic mantle source, in which the metasomes containing phlogopite, carbonate and clinopyroxene are responsible for the high-K and low silica. The high TiO_2 content (up to 6.25 wt%) also requires the involvement of phases such as titanomagnetite, titanite and perovskite, which are observed in Toro Ankole nodules (e.g., Link et al., 2008; Pitcavage et al., 2021). Apatite, also found as a rare mineral in some nodules, is a phase often associated with metasomatic, especially carbonatitic, events (Pitcavage et al., 2021). The presence of apatite in the source is required to explain the high P_2O_5 contents.

4.5. Open questions on ultramafic nodules

The compositions of the studied ultramafic nodules range from clinopyroxenite to glimmerite, with variable modal amounts of opaques and perovskite (Figs. EA10 a–c in Electronic Appendix 2). Calcite, commonly found as patches and as filling veins, is probably secondary (Figs. EA10 e–f in Electronic Appendix 2). Mineral chemical analyses highlight considerable overlap among phlogopites in one ultramafic nodule (from Bunyaruguru) and those found in the kamafugite lava in the same district. A similar compositional overlap has been also found for clinopyroxene, which is almost pure diopside. Link et al. (2008) identified three different generations of clinopyroxene in Toro Ankole nodules: the oldest are high Mg diopsides, found as colourless to pale green clinopyroxene cores, with a second generation of green rims. The third are euhedral to subhedral and larger green clinopyroxenes, with strong Ti enrichment, differing from the Al-rich nature of the previous rims.

The presence of similar nodules is widely reported in the WEAR (e.g., Lloyd, 1981, 1987; Barker and Nixon, 1989; Link et al., 2008; Muravyeva et al., 2014; Pitcavage et al., 2021). Foley's unpublished data on ultramafic nodules from Toro Ankole on a large set of samples (~600) indicate the main mineral phases as, in order of abundance, phlogopite, clinopyroxene, titanite, titanomagnetite, perovskite, apatite, carbonate, rarer feldspars and Cr-spinel. A question that remains unsolved despite decades of investigations is whether they should be considered as witness of the mantle source or as cumulates originating from previous similar magma batches. Some have been interpreted as related to metasomatic processes replacing previous peridotites (Lloyd and Bailey 1975), whereas other interpretations, which better fit the ultramafic nodules analysed in this study, favour magmatic and cumulate events (Lloyd, 1981, 1987). Nevertheless, even if their origin is still not clear, they point out that mantle beneath the Toro Ankole province is far from the classical anhydrous four-phase peridotite assemblage, reflecting a prolonged history of metasomatic changes.

Melting experiments at 1225–1250 °C and 3 GPa on a phlogopite-bearing clinopyroxenite produced melts with compositions similar to the kamafugite lavas of the Bunyaruguru and in the Katwe-Kikorongo volcanic district, allowing Lloyd et al. (1985) to interpret them as the mantle source of the ultrapotassic, moderately ultrabasic rocks cropping out in the northern WEAR.

Geochemical data (Fig. 5) point out a slightly different trend among the ultramafic nodules and the moderately ultrabasic lavas. Isotopic data of the ultramafic nodules reported here show a good agreement with results obtained for the kamafugitic samples and with published values from Toro Ankole field (Fig. 9a). The only exception are $^{206}Pb/^{204}Pb$ isotopic ratios (Fig. 10a and 10c) which show a slightly higher enrichment in the ultramafic nodules. Radiogenic Sr isotopic data could point to a phlogopite-rich source,

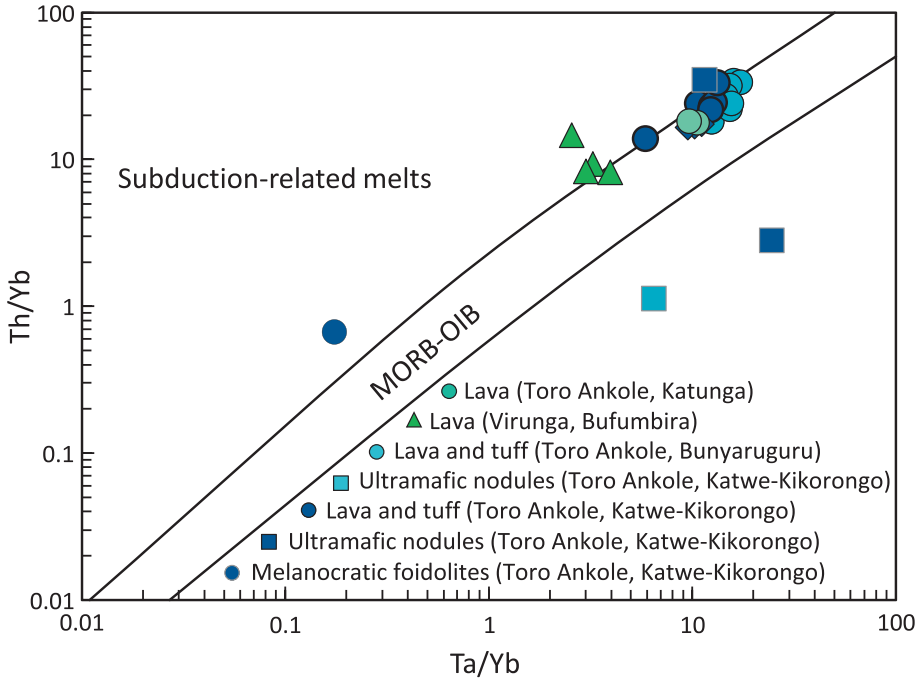

Fig. 14. Th/Yb vs. Ta/Yb diagram of the volcanic products, the ultramafic nodules and the melanocratic foidolites from Toro Ankole and Virunga volcanic provinces.

as for kamafugites, and the presence of recycled AOC + sediments. Seafloor altered materials, characterized by high Sr and B ratios, could explain both the radiogenic $^{87}Sr/^{86}Sr$ and the positive $\delta^{11}B$ of ultramafic nodules.

Whole-rock chemistry and mineral chemistry data, as well as textural features of the nodules analysed in this study make more likely their cumulate origin, probably related to primitive melt batches similar to the moderately ultrabasic volcanic rocks. Fractional crystallization of primitive melts may result in ultramafic cumulates that have settled down during ascent or formed coated channels. Geophysical studies in the area of the WEAR report a decrease in S-wave velocity between 55 and 80 km that is interpreted as the result of an alteration of the lithospheric mantle by infiltrating melts or crystal mushes (Lindenfeld et al., 2012). New magma batches may have taken these in suspension when piercing the channels, bringing the cargo to the surface.

4.6. Bufumbira (Virunga) volcanic rocks

Virunga lavas have less extreme compositions than Toro Ankole samples, with chemical features halfway between those of Toro Ankole rocks and the South Kivu alkali basalts. Petrographic observations reveal the presence of two different rock series at Bufumbira: an olivine leucitite to basanite group, with variable amounts of plagioclase found only in the groundmass (168, 169, 171: Figs. EA9 c–d Electronic Appendix 2 2) and a more evolved plagioclase-rich group (samples 156 and 159), in which plagioclase is also found as phenocryst (Figs. EA9 a–b Electronic Appendix 2). Samples from Bufumbira have nepheline and leucite in all but one sample whereas they are totally devoid of kalsilite, melilite or perovskite. Mineral compositions of the main phases are similar in the two Bufumbira rock groups, except for olivine. Olivine from trachybasalt 159 is characterized by higher FeO, resulting in a lower Fo (Fo_{60-63}), whereas basanite 169 has a Fo_{84-88}. Clinopyroxene shows higher Al_2O_3 (2.55–6.79 wt%) than in the Toro Ankole moderately ultrabasic lavas (<2.55 wt%).

Bufumbira lavas are characterized by higher SiO_2 (43.54–56.97 wt%), a slightly lower content of alkalis (4.42–7-98 wt%), coupled with higher Na_2O (1.68–3.25 wt%) than Toro Ankole moderately ultrabasic lavas. Bufumbira also shows lower TiO_2, CaO, and CO_2 and higher Al_2O_3 than Toro Ankole (Electronic Appendix 5). The flat MREE/HREE trend, coupled with higher HREE enrichment compared to Toro Ankole volcanics (Lu = 0.19–0.33 and 0.08–0.28, respectively) supports the absence of residual garnet in the Bufumbira mantle source.

Bufumbira lavas show more radiogenic $^{87}Sr/^{86}Sr$ (0.705805–0.707083) and less radiogenic $^{143}Nd/^{144}Nd$ (0.5123531–0.5124889) than Toro Ankole rocks. The negative Sr-B isotope correlation observed for these products could indicate the influence of recycled materials in the mantle source characterized by a ^{87}Sr-rich and ^{11}B-poor signature, such as siliciclastic sediments (Fig. 11b). Compared to moderately ultrabasic products from Toro Ankole, Bufumbira compositions are displaced towards the EMII end-member, in agreement with literature data (Bell and Powell, 1969; Vollmer and Norry, 1983). All these lines of evidence suggest modification of the sub-lithospheric mantle conditions, moving southward from Toro Ankole, with a less pronounced metasomatism in Virunga. All these features highlight that Bufumbira samples require a non-peridotite assemblage, with the possible presence of amphibole instead of phlogopite as the main hydrous phase, to explain the Na_2O increase and higher Na_2O/K_2O ratios (Rosenthal et al., 2009). Literature studies suggested an old metasomatic event for the Bufumbira mantle source, which would have generated a peridotite containing phlogopite ± amphibole ± clinopyroxene ± ilmenite ± rutile (Rogers et al., 1992). Based on Sr and Nd isotopic ratios, Vollmer and Norry (1983) proposed a refertilization event at ~500 Ma, whereas Rogers et al. (1992) favoured an older phase at ~1 Ga. These ages may be consistent with the recycling of crustal material during the Pan-African orogeny (Pitcavage et al., 2021).

Further detailed studies are required to achieve a better understanding of the processes and a better characterization of the metasomatic agents. Fig. 14 illustrates the different nature of the metasomatic agents that could have affected the sub-lithospheric mantle beneath Toro Ankole and Virunga. Virunga data plots towards slightly enriched compositions, also characterized by a higher degree of partial melting. Indeed, Bufumbira lavas straddle ratios between the mantle array and the subduction related fields, showing slightly lower Th/Yb and Ta/Yb ratios than Toro Ankole, which probably outlines the involvement of terrigenous sediments rather than AOC and limestone materials.

5. Concluding remarks

A comprehensive study based on petrographic, mineral chemical, geochemical and isotopic analyses highlights that the uncommon lithologies typical of Toro Ankole, such as melilitites, kamafugites and carbonatites indicate a complex and prolonged magmatic evolution and that extensive metasomatism affected the mantle sources. The high-K and silica-deficient compositions of the Toro Ankole rocks imply the presence of metasomes rich in phlogopite and carbonates in the mantle. In order to explain all the geochemical (low SiO_2, high TiO_2, CaO and K_2O together with the high LILE), mineral chemical and isotopic (radiogenic $^{87}Sr/^{86}Sr$) features, the paragenesis of the metasomatic veins additionally require clinopyroxene, titanite and apatite. This source assemblage would be supported by the primitive incompatible element patterns and results to be similar to the ultramafic nodules found in the volcanic products. Nevertheless, the actual nature of such nodules is still debated, representing another 'chicken or egg' dilemma. Melting of these metasomes, which have a liquidus temperatures lower than four-phase peridotite, would result in silica-poor and CaO-rich melts.

Results from this study confirm a variation trend in the WEAR in which more intense metasomatism involving a moderately ^{87}Sr-enriched and ^{11}B-rich component such as AOC and carbonate sediments occurred at Toro Ankole in the northern region of the WEAR than at Virunga further south. The southward decrease of K_2O/Na_2O ratios from Toro Ankole to Virunga, South Kivu and Rungwe suggests a change from a phlogopite-dominated to pargasite-dominated melting assemblage (Rosenthal et al., 2009; Foley et al., 2012). The wider participation of amphibole in the mantle source of Bufumbira products would also be consistent with a slightly lower depth of melting (e.g., Pitcavage et al., 2021), which become much shallower southward (e.g., 65 km in the Rungwe Volcanic Province; Furman and Graham, 1999).

CRediT authorship contribution statement

Francesca Innocenzi: Investigation, Visualization, Data curation, Writing - original draft. **Sara Ronca:** Investigation, Writing - review & editing. **Stephen Foley:** Conceptualization, Resources, Writing - review & editing. **Samuele Agostini:** Investigation, Resources, Writing - review & editing. **Michele Lustrino:** Conceptualization, Resources, Writing - review & editing.

Declaration of Competing Interest

The authors declare that they have no known competing financial interests or personal relationships that could have appeared to influence the work reported in this paper.

Acknowledgments

The authors warmly thank Domenico Mannetta for his help during thin sections production, Marco Albano and Tania Ruspandini for the analyses at the scanning electron microscope. A very special thank goes to Marcello Serracino, who kept in perfect function for 32 years the glorious Cameca SX 50, which was dismantled just after the mineral chemistry analyses presented here.

The detailed reviews of Vladislav Rapprich (Praha, Czech Republic) and Igor Ashchepkov (Novosibirsk, Russia) greatly improved the quality of the paper. The authors thank the Editor Li Tang for the scientific handling. This work was financially supported by Sapienza Ateneo grants (2020, 2021) to ML and IGG-CNR-P0CT0061 funding to SA. FI is grateful to Irene Cornacchia for sharing her knowledge on continental carbonates and for her help in IGG laboratories. She also thanks Nicola for his invaluable support.

Appendix A. Supplementary material

Supplementary data to this article can be found online at https://doi.org/10.1016/j.gr.2023.09.005.

References

Afonso, J.C., Ben-Mansour, W., O'Reilly, S.Y., Griffin, W.L., Salajeghegh, F., Foley, S., Begg, G., Selway, K., Macdonald, A., Januszczak, F.I., Nyblade, A.A., Yang, Y., 2022. Thermochemical structure and evolution of cratonic lithosphere in central and southern Africa. Nat. Geosci. 15, 405–410.

Agostini, S., Di Giuseppe, P., Manetti, P., Doglioni, C., Conticelli, S., 2021. A heterogeneous subcontinental mantle under the African-Arabian Plate boundary revealed by boron and radiogenic isotopes. Sci. Rep. 11, 11230. https://doi.org/10.1038/s41598-021-90275-7.

Andersen, T., Elburg, M., Erambert, M., 2012. Petrology of combeite-and götzenite-bearing nephelinite at Nyiragongo, Virunga Volcanic Province in the East African Rift. Lithos 152, 105–121.

Aoki, K.I., Yoshida, T., Yusa, K., Nakamura, Y., 1985. Petrology and geochemistry of the Nyamuragira volcano. Zaire. J. Volcanol. Geotherm. Res. 25, 1–28.

Arima, M., Edgar, A.D., 1983. High pressure experimental studies on a katungite and their bearing on the genesis of some potassium-rich magmas of the west branch of the African rift. J. Petrol. 24, 166–187.

Auchapt, A., Dupuy, C., Dostal, J., Kanika, M., 1987. Geochemistry and petrogenesis of rift-related volcanic rocks from South Kivu (Zaire). J. Volcanol. Geoth. Res. 31, 33–46.

Barette, F., Poppe, S., Smets, S., Benbakkar, M., Kervyn, M., 2017. Spatial variation of volcanic rock geochemistry in the Virunga Volcanic Province: Statistical analysis of an integrated database. J. African Earth Sci. 134, 888–903.

Barifaijo, E., Muwanga, A., Schumann, A., 2010. Geochemistry of the potassic basalts from the Bufumbira volcanic field in southwestern Uganda. Tanz. J. Sci. 36, 95–112.

Barker, D.S., 2007. Origin of cementing calcite in "carbonatite" tuffs. Geol. Soc. Am. 35, 371–374.

Barker, D.S., Nixon, P.H., 1989. High-Ca, low-alkali carbonatite volcanism at Fort Portal, Uganda. Contrib. Mineral. Petrol. 103, 166–177.

Barrière, J., d'Oreye, N., Smets, B., Oth, A., Delhaye, L., Subira, J., Mashagiro, N., Derauw, D., Smittarello, D., Muhindo Syavulisembo, A., Kervyn, F., 2022. Intra-crater eruption dynamics at Nyiragongo (DR Congo), 2002–2021. J. Geophy. Res.: Solid Earth 127, e2021JB023858.

Bell, K., Doyle, R.J., 1971. K-Rb relationships in some continental alkalic rocks associated with the East African Rift Valley System. GCA 35, 903–915.

Bell, K., Powell, J.L., 1969. Strontium Isotopic Studies of Alkalic Rocks: The Potassium-rich Lavas of the Birunga and Toro Ankole Regions, East and Central Equatorial Africa. J. Petrol. 10, 536–572.

Boudoire, G., Giuffrida, G., Liuzzo, M., Bobrowki, N., Calabrese, S., Kuhn, J., Kazadi Mwepu, J.-C., Grassa, F., Caliro, S., Rizzo, A.L., Italiano, F., Yalire, M., Karume, K., Muhindo, S.A., Tedesco, D., 2022. Chemical variability in volcanic gas plumes and fumaroles along the East African Rift System: new insights from the western branch. Chem. Geol. 596, 120811.

Brand, U., Veizer, J., 1980. Chemical diagenesis of a multicomponent carbonate system; 1, Trace elements. J. Sediment. Res. 50, 1219–1236.

Brod, J.A., Gibson, S.A., Thompson, R.N., Junqueira-Brod, T.C., Seer, H.J., De Moraes, L. C., Boaventura, G.R., 2000. The kamafugite-carbonatite association in the Alto Paranaíba Igneous Province (APIP) southeastern Brazil. Rev. Bras. Geociênc. 30, 408–412.

Brooker, R.A., Kjarsgaard, B.A., 2011. Silicate-carbonate liquid immiscibility and phase relations in the system SiO_2-Na_2O-Al_2O_3-CaO-CO_2 at 0.1–2.5 GPa with applications to carbonatite genesis. J. Petrol. 52, 1281–1305.

Capaccioni, B., Yalire, M.M., Santo, A.P., Vaselli, O., 2002. Monogenic and polygenic volcanoes in the area between the Nyiragongo summit crater and the Lake Kivu shoreline, Monogenic and polygenic volcanoes between Nyiragongo and Lake Kivu. Acta Vulcanol. 14, 129–136.

Chakhmouradian, A.R., 2006. High-field-strength elements in carbonatitic rocks: geochemistry, crystal chemistry and significance for constraining the sources of carbonatites. Chem. Geol. 235, 138–160.

Chakrabarti, R., Basu, A.R., Santo, A.P., Tedesco, D., Vaselli, O., 2009. Isotopic and geochemical evidence for a heterogeneous mantle plume origin of the Virunga volcanics, Western rift, East African Rift system. Chem. Geol. 259, 273–289.

Chaussidon, M., Albarède, F., 1992. Secular boron isotope variations in the continental crust: an ion microprobe study. Earth Planet. Sci. Lett. 108, 229–241.

Chorowicz, J., 2005. The East African rift system. J. African Earth Sci. 43, 379–410.

Combe, A., Holmes, A., 1945. The kalsilite bearing lavas of Kabirenge and Lyakauli, South-West Uganda. Trans. R. Soc. Edinb. 41, 359–379.

Condomines, M., Carpentier, M., Ongendangenda, T., 2015. Extreme radium deficit in the 1957 AD Mugogo lava (Virunga volcanic field, Africa): Its bearing on olivine-melilitite genesis. Contrib. Mineral. Petrol. 169, 29.

Dawson, J.B., 1989. Sodium carbonatite extrusions from Oldoinyo Lengai, Tanzania: Implications for carbonatite complex genesis. In: Bell, K. (Ed.), Carbonatites: Genesis and Evolution. Unwin Hyman, London, pp. 255–277.

De Mulder, M., Pasteels, P., 1986. K-Ar geochronology of the Karisimbi volcano (Virunga, Rwanda - Zaire). J. African Earth Sci. 5, 575–579.

De Waele, B., Johnson, S.P., Pisarevsky, S.A., 2008. Paleoproterozoic to Neoproterozoic growth and evolution of the eastern Congo Craton. Its role in the Rodenia puzzle. Precambr. Res. 160, 127–141.

Demant, A., Lestrade, P., Lubala, R.T., Kampunzu, A.B., Durieux, J., 1994. Volcanological and petrological evolution of Nyiragongo volcano, Virunga volcanic field. Zaire. Bull. Volcanol. 56, 47–61.

Denaeyer, M.E., 1956. La nouvelle éruption du Nyamulagira. Bull. Acad. Roy. Sci. Coloniales 2, 1226–1228.

Denaeyer, M.E., 1960. Composition de la lave actuelle du Nyiragongo et de quelques laves similaires de ce volcan. Bull. Acad. Roy. Sci. Outre-Mer 6, 999–1013.

Denaeyer, M.E., 1965. Recueil d'analyses des laves du fosse tectonique de l'Afrique Centrale (Kivu, Rwanda, Toro-Ankole). Ann. Mus. Roy. Afrique Central Tervuren (Belgique), Ser. Geol. 49, 234.

Denaeyer, M.E., Tazieff, H., Pruvost, P., 1957. Nature de la lave actuelle et de quelques laves plus anciennes de la caldère du Nyiragongo (Kivu). C.R. Hebdomadaires Acad. Sci. 244, 218–221.

Denaeyer, M.E., 1972. Les laves du fosse tectouique de l'Afrique Centrale (Kivu, Rwanda, Toro Ankole). I. Supplement au recueil d'analyses de 1965. II. Magmatologie. Ann. Mus. Roy. Afrique Cent., Tervuren, Belgique: Annales Série In-8 Sciences Geologiques, 72–134.

Ebinger, C.J., 1989. Tectonic development of the western branch of the East-African rift system. Geol. Soc. Am. Bull. 101, 885–903.

Ebinger, C.J., Deino, A.L., Drake, R.E., Tesha, A.L., 1989. Chronology of volcanism and rift basin propagation: Rungwe volcanic province, East Africa. J. Geophys. Res. 94, 15785–15803.

Eby, G.N., Lloyd, F.E., Woolley, A.R., 2009. Geochemistry and petrogenesis of the Fort Portal, Uganda, extrusive carbonatite. Lithos 113, 785–800.

Edgar, A.D., Vukadinovic, D., 1992. Implications of experimental petrology to the evolution of ultrapotassic rocks. Lithos 28, 205–220.

Finckh, L., 1912. Die Jungvulkanischen Gesteine des Kiwusee-gebietes. Wiss. Ergebn. d. Deutsch. Zentral-Africa Exped. 1097–1908 (1), 1–44.

Flügel, E., 2004. Microfacies data: fabrics. In: Microfacies of Carbonate Rocks. Springer, Berlin.

Foley, S.F., 1992. Vein-plus-wall-rock melting mechanisms in the lithosphere and the origin of potassic alkaline magmas. Lithos 28, 435–453.

Foley, S.F., Pintér, Z., 2018. Primary melt compositions in the Earth's mantle. In: Magmas Under Pressure. Elsevier, pp. 3–42.

Foley, S.F., Venturelli, G., Green, D.H., Toscani, L., 1987. The ultrapotassic rocks: characteristics, classification, and constraints for petrogenetic models. Earth Sci. Rev. 24, 81–134.

Foley, S.F., Jacob, D.E., O'Neill, H.S.C., 2011. Trace element variations in olivine phenocrysts from Ugandan potassic rocks as clues to the chemical characteristics of parental magmas. Contrib. Mineral. Petrol. 162, 1–20.

Foley, S.F., Link, K., Tiberindwa, J.V., Barifaijo, E., 2012. Patterns and origin of igneous activity around the Tanzanian craton. J. African Earth Sci. 62, 1–18.

Fontijn, K., Williamson, D., Mbede, E., Ernst, G.G., 2012. The Rungwe volcanic province, Tanzania–a volcanological review. J. African Earth Sci. 63, 12–31.

Furman, T., 1995. Melting of metasomatized subcontinental lithosphere: undersatured mafic lavas of Rungwe, Tanzania. Contrib. Mineral. Petrol. 122, 97–115.

Furman, T., Graham, D., 1999. Erosion of lithospheric mantle beneath the East African Rift system" geochemical evidence from the Kivu volcanic province. Lithos 48, 237–262.

Furman, T., Kaleta, K.M., Bryce, J.G., Hanan, B.B., 2006. Tertiary Mafic Lavas of Turkana, Kenya: Constraints on East African Plume Structure and the Occurrence of High-m Volcanism in Africa. J. Petrol. 47, 1221–1244.

Gargiulo, M.F., Bjerg, E.A., Mogessie, A., 2013. Spinel group minerals in metamorphosed ultramafic rocks from Río de Las Tunas belt, Central Andes, Argentina. Geol. Acta 11, 133–148.

Gozzi, F., Gaeta, M., Freda, C., Mollo, S., Di Rocco, T., Marra, F., Dallai, L., Pack, A., 2014. Primary magmatic calcite reveals origin from crustal carbonate. Lithos 190–191, 191–203.

Guibert, P., Delaloye, M., Hunziker, J., 1975. Contribution a l'etude geologiques du volcan Mikeno, Chaîne des Virunga Republique du Zaïre. Compte Rendu des Seances de la Societe de Physique d'Histoire Naturelle de Geneve 10, 57–66.
Guzmics, T., Zajacz, Z., Mitchell, R.H., Szabó, C., Wälle, M., 2015. The role of liquid–liquid immiscibility and crystal fractionation in the genesis of carbonatite magmas: insights from Kerimasi melt inclusions. Contrib. Mineral. Petrol. 169, 1–18.
Hart, S.R., 1984. A large-scale isotope anomaly in the southern hemisphere mantle. Nature 309, 753–757.
Hertogen, J., Vanlerberghe, L., Namegabe, M.R., 1985. Geochemical evolution of the Nyiragongo volcano (Virunga, Western African Rift, Zaire). Bull. Geol. Soc. Finland 57, 21–35.
Higazy, R.A., 1954. Trace elements of volcanic ultrabasic potassic rocks of southwestern Uganda and adjoining part of the Belgian Congo. Geol. Soc. Am. Bull. 65, 39–70.
Holmes, A., 1936. Transfusion of quartz xenoliths in alkali basic and ultrabasic lavas, south-west Uganda. Mineral. Mag. 24, 408–421.
Holmes, A., 1937. The petrology of katungite. Geol. Mag. 74, 200–219.
Holmes, A., 1942. A suite of volcanic rocks from south-west Uganda containing kalsilite (a polymorph of KAlSiO4). Mineral. Mag. 26, 197–217.
Holmes, A., 1950. Petrogenesis of katungite and its associates. Am. Min. 35, 772–792.
Holmes, A., 1952. The potash ankaratrite-mela-leucitites lavas from Nabugando and Mbuga craters, South/West Uganda. Trans. R. Soc. Edinb. 15, 187–213.
Holmes, A., 1956. The ejectamenta of Katwe Crater, South-west Uganda: Verhandel. Koninkl. Ned. geol. Mijnbouwk Genoot. 16, 1–28.
Holmes, A., Harwood, H.F., 1932. Petrology of the volcanic fields east and south-east of Ruwenzori, Uganda. Quar. J. Geol. Soc. 88, 370–442.
Holmes, A., Harwood, H.F., 1936. The volcanic area of Bufumbira. Part II. Mem. Geol. Surv. Ug. 3, 300.
Holmes, A., Harwood, H.F., 1937. The volcanic area of Bufumbira. Geol. Fören. Stockh. Förh. 59, 362–363.
Hulett, S.R., Simonetti, A., Rasbury, E.T., Hemming, N.G., 2016. Recycling of subducted crustal components into carbonatite melts revealed by boron isotopes. Nat. Geosci. 9, 904–908.
Innocenzi, F., Ronca, S., Foley, S.F., Agostini, S., Lustrino, M., 2022. Exotic magmatism from the western branch of the East African Rift: insights on the lithospheric mantle source. EGU General Assembly, Vienna, Austria, 23–27 May 2022, EGU22-5450. doi: 10.5194/egusphere-egu22-5450.
Innocenzi, F., Ronca, S., Agostini, S., Brandano, M., Caracausi, A., Lustrino, M., 2021. The pyroclastic breccias from Cabezo Negro de Tallante (SE Spain): Is there any relation with carbonatitic magmatism? Lithos 392, 106140.
Jess, S., Koehn, D., Fox, M., Enkelmann, E., Sachau, T., Aanyu, K., 2020. Paleogene initiation of the Western Branch of the East African Rift: Theuplift history of the Rwenzori Mountains, Western Uganda. Earth Planet. Sci. Lett. 552, 116593.
Kampunzu, A.B., Mohr, P., 1991. Magmatic evolution and petrogenesis in the East African Rift system. In: Kampunzu, A.B., Lubala, R.T. (Eds.), Magmatism in Extensional Structural Settings: the Phanerozoic African Plate. Springer, Berlin, pp. 85–136.
Kelemen, P.B., Manning, C.E., 2015. Reevaluating carbon fluxes in subduction zones, what goes down, mostly comes up. Proc. Nat. Acad. Sci. 112, E3997–E4006.
King, S., Anderson, D.L., 1998. Edge-driven convection. Earth Planet. Sci. Lett. 160, 289–296.
King, A.J., Phillips, K.J.H., Strekopytov, S., Vita-Finzi, C., Russell, S.S., 2020. Terrestrial modification of the Ivuna meteorite and a reassessment of the chemical composition of the CI type specimen. GCA 268, 73–89.
Krmíček, L., Chalapathi Rao, N.V., 2021. Lamprophyres, lamproites and related rocks as tracers to supercontinent cycles and metallogenesis. Geol. Soc. Lond., Spec. Publ. 513, 474.
Lacroix, A., 1923. Min. Madagascar, 3, 267 pp.
Lawrence, L., Spandler, C., Hilbert-Wolf, H.L., Mtelela, C., Stevens, N.J., O'Connor, P. M., Roberts, E.M., 2022. Radiogenic isotope record of magma genesis and lithospheric geodynamics of the Rukwa Rift Basin, Tanzania, from mid Mesozoic to present. Chem. Geol. 608, 121040.
Le Maitre, R.W., 2002. Classification of Igneous Rocks and Glossary of Terms. Recommendations of the IUGS subcommission on the systematics of igneous rocks. Cambridge University Press.
Lindenfeld, M., Rümpker, G., Link, K., Koehn, D., Batte, A., 2012. Fluid-triggered earthquake swarms in the Rwenzori region, East African Rift—Evidence for rift initiation. Tectonophysics 566, 95–104.
Link, K., Barifaijo, E., Tiberindwa, J., Foley, S.F., 2008. Veined pyroxenite xenoliths from the kamafugites in the Toro Ankole region of western Uganda: a window to a rift-related mantle. 9th International Kimberlite Conference Extended Abstract.
Link, K., Koehn, D., Barth, M.G., Tiberindwa, J.V., Barifaijo, E., Aanyu, K., Foley, S.F., 2010. Continuous cratonic crust between the Congo and Tanzania blocks in western Uganda. Int. J. Earth Sci. 99, 1559–1573.
Lloyd, F.E., 1981. Upper-mantle metasomatism beneath a continental rift: clinopyroxenes in alkali mafic lavas and nodules from South West Uganda. Mineral. Mag. 44, 315–323.
Lloyd, F.E., 1985. Experimental melting and crystallisation of glassy olivine melilitites. Contrib. Mineral. Petrol. 90, 236–243.
Lloyd, F.E., 1987. Characterisation of mantle metasomatic fluids in spinel lherzolites and alkali clinopyroxenites from the West Eifel and South West Uganda. In: Menzies, M., Hawkesworth, C.J. (Eds.), Mantle Metasomatism. Academic Press, London, pp. 91–123.
Lloyd, F.E., Bailey, D., 1975. Light element metasomatism of the continental mantle: the evidence and the consequences. In: Physics and Chemistry of the Earth. Physics and Chemistry of the Earth, pp. 389–416.
Lloyd, F.E., Arima, M., Edgar, A.D., 1985. Partial melting of a phlogopite-clinopyroxenite nodule from south-west Uganda: an experimental study bearing on the origin of highly potassic continental rift volcanics. Contrib. Mineral. Petrol. 91, 321–329.
Lustrino, M., Pistocchi, L., Ronca, S., Innocenzi, F., Agostini, S., 2022a. Carbonate assimilation of ultrabasic magma: the Pleistocene Cupaello kamafugitic volcano (central Italy). EGU General Assembly, Vienna, Austria, 23–27 May 2022, EGU22-5673. doi: 10.5194/egusphere-egu22-5673.
Lustrino, M., Fedele, L., Agostini, S., Prelević, D., Salari, G., 2019a. Leucitites within and around the Mediterranean area. Lithos 324, 216–233.
Lustrino, M., Luciani, N., Stagno, V., 2019b. Fuzzy petrology in the origin of carbonatitic/pseudocarbonatitic Ca-rich ultrabasic magma at Polino central Italy. Sci. Rep. 9, 1–14.
Lustrino, M., Ronca, S., Caracausi, A., Ventura, Bordenca, C., Agostini, S., Faraone, D. B., 2020. Strongly SiO2-undersaturated, CaO-rich kamafugitic Pleistocene magmatism in Central Italy (San Venanzo volcanic complex) and the role of shallow depth limestone assimilation. Earth Sci. Rev. 208, 103256.
Lustrino, M., Luciani, N., Stagno, V., Narzisi, S., Masotta, M., Scarlato, P., 2022b. Experimental evidence on the origin of Ca-rich carbonated melts formed by interaction between sedimentary limestones and mantle-derived ultrabasic magmas. Geology 50, 476–480.
Lyubetskaya, T., Korenaga, J., 2007. Chemical composition of Earth's primitive mantle and its variance: 1. Method and results. J. Geophys. Res. 112, 1–21.
Mafuko Nyandwi, B., Kervyn, M., Habiyaremye, M., Kervyn, F., Michellier, C., 2022. Differences in volcanic risk perception among Goma's population before the Nyiragongo eruption of May 2021, Virunga volcanic province DR Congo. Natural Hazards and Earth System Sciences. doi: 10.5194/nhess-2022-217 (in press).
Marcelot, G., Rançon, J.P., 1988. Mineral chemistry of leucitites from Visoke Volcano (Virunga Range, Rwanda): petrogenetic implications. Mineral. Mag. 52, 603–613.
Marcelot, G., Rançon, J.P., Demange, J., 1985. The potassic series of Karisimbi volcano (Virunga Range, Rwanda): volcanological and petrological aspects. J. Volcanol. Geoth. Res. 26, 99–129.
Marcelot, G., Dupuy, C., Dostal, J., Rancon, J.P., Pouclet, A., 1989. Geochemistry of mafic volcanic rocks from the Lake Kivu (Zaire and Rwanda) section of the western branch of the African Rift. J. Volcanol. Geoth. Res. 39, 73–88.
Marschall, H.R., 2018. Boron Isotopes in the Ocean Floor Realm and the Mantle. In: Marschall, H., Foster, G. (Eds.), Boron Isotopes. Advances in Isotope Geochemistry. Springer, Cham. https://doi.org/10.1007/978-3-319-64666-4_8.
Martin, L.H., Schmidt, M.W., Mattsson, H.B., Guenther, D., 2013. Element partitioning between immiscible carbonatite and silicate melts for dry and H_2O-bearing systems at 1–3 GPa. J. Petrol. 54, 2301–2338.
Melluso, L., Lustrino, M., Ruberti, E., Brotzu, P., De Barros Gomes, C., Morbidelli, L., Morra, V., Svisero, D.P., d'Amelio, F., 2008. Major and trace-element compositions of olivine, perovskite, clinopyroxene, Cr-Fe-Ti oxides, phlogopite and host kamafugites and kimberlites, Alto Paranaiba, Brazil. Can. Mineral. 46, 19–40.
Mesko, G.T., 2020. Magmatism at the southern end of the East African rift system: Origin and role during early stage rifting. Phd Thesis, Columbia University.
Michon, L., Famin, V., Quidelleur, X., 2022. Evolution of the East African Rift System from trap-scale to plate-scale rifting. Earth Sci. Rev. 231, 104089.
Minissale, S., 2017. Petrogenesis of alkaline and strongly alkaline volcanism: examples from African Rift. University of Naples, Federico II. Unpublished PhD thesis.
Minissale, S., Zanetti, A., Tedesco, D., Morra, V., Melluso, L., 2019. The petrology and geochemistry of Nyiragongo lavas of 2002, 2016, 1977 and 2017 AD, and the trace element partitioning between melilitite glass and melilite, nepheline, leucite, clinopyroxene, apatite, olivine and Fe-Ti oxides: a unique scenario. Lithos 332, 296–311.
Minissale, S., Casalini, M., Cucciniello, C., Balagizi, C., Tedesco, D., Boudoire, G., Morra, V., Melluso, L., 2022. The geochemistry of recent Nyamulagira and Nyiragongo potassic lavas, Virunga Volcanic Province, and implications on the enrichment processes in the mantle lithosphere of the Tanzania-Congo craton. Lithos, 106696.
Mitchell, R.H., 2020. Igneous rock associations 26. Lamproites, exotic potassic alkaline rocks: a review of their nomenclature, characterization and origins. Geosci. Can. 47, 119–142.
Mitchell, R.H., Bell, K., 1976. Rare earth element geochemistry of potassic lavas from the Birunga and Toro Ankole regions of Uganda, Africa. Contrib. Mineral. Petrol. 58, 293–303.
Mitchell, R.H., Gittins, J., 2022. Carbonatites and carbothermalites: a revised classification. Lithos 430–431, 106861.
Morimoto, N., 1989. Nomenclature of pyroxene. Can. Mineral. 27, 143–156.
Mulder, M., Hertogen, J., Deutsch, S., André, L., 1986. The role of crustal contamination in the potassic suite of the Karisimbi volcano Virunga, African Rift Valley. Chem. Geol. 57, 117–136.
Murav'eva, N.S., Senin, V.G., 2009. Carbonate-silicate equilibria in the high-magnesia ultrapotassic volcanics of the Toro Ankole Province Eastern African rift zone. Geochem. Int. 47, 882–900.
Muravyeva, N.S., Belyatsky, B.V., Senis, V.G., Ivanov, A.V., 2014. Sr–Nd–Pb isotope systematics and clinopyroxene-host disequilibrium in ultra-potassic magmas from Toro Ankole and Virunga, East-African Rift: Implications for magma mixing and source heterogeneity. Lithos 210–211, 260–277.

Muravyeva, N.S., Senin, V.G., Ivanov, A.V., Belyatsky, B.V., 2021. Leucite basanites of Virunga (East African Rift): some insights into petrogenesis and source composition. Lithos 384–385, 105972.
Nakamura, Y., Aoki, K., 1980. The 1977 eruption of Nyiragongo volcano, eastern Africa, and chemical composition of the ejecta. Bull. Volcanol. Soc. Jpn. 25, 17–32.
Nixon, P.H., Hornung, G., 1973. The carbonatite lavas and tuffs near Fort Portal, western Uganda. Overseas Geol. Mineral. Resour. 41, 168–179.
Novella, D., Keshav, S., Gudfinnsson, G.H., Ghosh, S., 2014. Melting phase relations of model carbonated peridotite from 2 to 3 GPa in the system CaO-MgO-Al_2O_3-SiO_2-CO_2 and further indication of possible unmixing between carbonatite and silicate liquids. J. Geophys. Res. 119, 2780–2800.
Ödman, O.H., 1930. Volcanic Rocks of Mt. Elgon in British East Africa. Geol. Fören. Stockh. Förh. 3, 455–537.
Oliveira, I.L., Brod, J.A., Junqueira-Brod, T.C., Reimold, W.U., Fuck, R.A., 2022. The IUGS nomenclature on kalsilite-bearing volcanic rocks: a critical appraisal and reccomendations. J. Petrol. 63, 1–14.
Pickett, D.A., Murrell, M.T., 1997. Observations of $^{231}Pa/^{235}U$ disequilibrium in volcanic rocks. Earth Planet. Sci. Lett. 148, 259–271.
Pitcavage, E., Furman, T., Nelson, W., Kalegga, P.K., Barifaijo, E., 2021. Petrogenesis of primitive lavas from the Toro Ankole and Virunga Volcanic Provinces: Metasomatic mineralogy beneath East Africa's Western Rift. Lithos 106192.
Platz, T., Foley, S.F., André, L., 2004. Low-pressure fractionation of the Nyiragongo volcanic rocks, Virunga Province, D.R. Congo. J. Volcanol. Geotherm. Res. 136, 269–295.
Pouclet, A., 1973. Contribution à la connaissance du Volcan Nyiragongo (Rift ouest-africain) Les éruptions intra-cratèrales de juillet 1971 à avril 1972. Bull. Volcanol. 37, 37–72.
Pouclet, A., Ménot, R.P., Piboule, M., 1983. Le magmatisme alcalin potassique de l'aire volcanique des Virunga (Rift occidental de l'Afrique de l'Est). Une approche statistique dans la recherche des filiations magmatiques et des mécanismes de différenciation. Bull. Mineral. 106, 607–622.
Pouclet, A., Menot, R.P., Piboule, M., 1984. Differenciation des laves de l'Afrique Centrale (Rift Ouest). Contribution de l'analyse statistique multivariee. Neues Jb. Miner. Abh. 149, 283–308.
Pouclet, A., Bellon, H., Bram, K., 2016. The Cenozoic volcanism in the Kivu rift: Assessment of the tectonic setting, geochemistry, and geochronology of the volcanic activity in the South-Kivu and Virunga regions. J. African Earth Sci. 121, 219–246.
Rapprich, V., Vladimír, Ž., Kryštof, V., Vojtěch, E., Tomasz, G., Yewubinesh, B., Firdawok, L., Tomáš, H., Petra, H., 2016. Wendo Koshe Pumice: The latest Holocene silicic explosive eruption product of the Corbetti volcanic system (southern Ethiopia). J. Volcanol. Geoth. Res. 310, 159–171.
Roberts, E.M., Stevens, N.J., O'Connor, P.M., Dirks, P.H.G.M., Gottfried, M.D., Clyde, W.C., Armstrong, R.A., Kemp, I.S., Hemming, S., 2012. Initiation of the western branch of the East African Rift coeval with the eastern branch. Nat. Geosci. 5, 289–294.
Rogers, N.W., De Mulder, M., Hawkesworth, C.J., 1992. An enriched mantle source for potassic basanites: evidence from Karisimbi volcano, Virunga volcanic province, Rwanda. Contrib. Mineral. Petrol. 111, 543–556.
Rogers, N.W., James, D., Kelley, S.P., De Mulder, M., 1998. The generation of potassic lavas from the eastern Virunga province, Rwanda. J. Petrol. 39, 1223–1247.
Rooney, T.O., 2017. The Cenozoic magmatism of East-Africa: Part I—Flood basalts and pulsed magmatism. Lithos 286, 264–301.
Rooney, T.O., 2020a. The Cenozoic magmatism of East Africa: Part II–Rifting of the mobile belt. Lithos 360, 105291.
Rooney, T.O., 2020b. The Cenozoic magmatism of East Africa: part III–rifting of the craton. Lithos 360, 105390.
Rosenthal, A., Foley, S.F., Pearson, D.G., Nowell, G.M., Tappe, S., 2009. Petrogenesis of strongly alkaline primitive volcanic rocks at the propagating tip of the western branch of the East African Rift. Earth Planet. Sci. Lett. 284, 236–248.
Sahama, T.G., 1953. Mineralogy and petrology of a lava flow from Mt. Nyiragongo, Belgian Congo. Ann. Acad. Sci. Fenn. 35, 1–25.
Sahama, T.G., 1957. Complex nepheline-kalsilite phenocrysts in Kabfumu lava, Nyiragongo area, North Kivu in Belgian Congo. J. Geol. 65, 515–526.
Sahama, T.G., 1962a. Petrology of Mt. Nyiragongo: a review. Trans. R. Soc. Edinb. 19, 1–28.
Sahama, T.G., 1974. Potassium-rich alkali rocks. In: Sørensen, H. (Ed.), The Alkaline Rocks. Wiley, London, pp. 96–109.
Sahama, T.G., Meyer, A., 1958. Study of the volcano Nyiragongo, a progress report. Inst. Parcs Nationaux Congo Belge, Mission d'Etudes Vulcanologiques J, Tervuren 2, 1–85.
Sahama, T.G., 1978. The Nyiragongo main cone. Musée Royale de l'Afrique Centrale, Tervuren, Belgique: Annales Série In-8 Sciences Geologiques, 81, 1–88.
Santo, A.P., Capaccioni, B., Tedesco, D., Vaselli, O., 2003. Petrographic and geochemical features of the 2002 Nyiragongo lava flows. Acta Vulcanol. 14, 63.
Schmidt, M.W., Weidendorfer, D., 2018. Carbonatites in oceanic hotspots. Geology 46, 435–438.
Scott Smith, B.H., Nowicki, T.E., Russel, J.K., Webb, K.J., Mitchell, R.H., Hetman, C.M., Robey, J. A., 2018. A glossary of Kimberlite and related terms. Scott Smith Petrology Inc., North Vancouver, BC, Canada. Part 1–144.
Smets, B., Kervyn, M., d'Oreye, N., Kervyn, F., 2015. Spatio-temporal dynamics of eruptions in a youthful extensional setting: Insights from Nyamulagira Volcano DR Congo, in the western branch of the East African Rift. Earth Sci. Rev. 150, 305–328.
Smith, W., 1931. A classification of some rhyolites, trachytes and phonolites from part of Kenya Colony, with a note on some associated basaltic rocks. Quart. J. Geol. Soc. 87, 212–258.
Stoppa, F., Schiazza, M., 2013. An overview of monogenetic carbonatitic magmatism from Uganda, Italy, China and Spain: volcanologic and geochemical features. J. S. Am. Earth Sci. 41, 140–159.
Stoppa, F., Woolley, A.R., Lloyd, F.E., Eby, N., 2000. Carbonatite lapilli-bearing tuff and a dolomite carbonatite bomb from Murumuli crater, Katwe volcanic field, Uganda. Mineral. Mag. 64, 641–650.
Tappe, S., Shaikh, A.M., Wilson, A.H., Stracke, A., 2022. Evolution of ultrapotassic volcanism on the Kaapvaal craton: deepening the orangeite versus lamproite debate. Geol. Soc. Lond. Special Publication. doi: 10.1144/SP513-2021-84 (in press).
Tappe, S., Foley, S.F., Pearson, D.G., 2003. The Kamafugites of Uganda: a mineralogical and geochemical comparison with their Italian and Brazilian analogues. Period. Mineral. 72, 51–77.
Thomas, R.J., Spencer, C., Bushi, A.M., Baglow, N., Boniface, N., de Cock, G., Horstwood, M.S.A., Hollick, L., Jacobs, J., Kajara, S., Kamihanda, G., Key, R.M., Maganga, Z., Mbawala, F., McCourt, W., Momburi, P., Moses, F., Mruma, A., Myambilwa, Y., Roberts, N.M.W., Saidi, H., Nyanda, P., Nyoka, K., Millar, I., 2016. Geochronology of the central Tanzania Craton and its southern and eastern orogenic margins. Precambr. Res. 277, 47–67.
Thompson, R.N., 1975. The 1-atmosphere liquidus oxygen fugacities of some tholeiitic intermediate, alkalic and ultra-alkalic lavas. Am. J. Sci. 275, 1049–1072.
Tilley, C.E., Thompson, R.N., 1972. Melting relations of some ultra-alkali volcanics. Geol. J. 8, 65–70.
Velasquez Ruiz, F., Cordeiro, P., Reich, M., Motta, J.B., Cordeiro Ribeiro, C., Angerer, T., Borges Bernardes, R., 2022. The genetic link between kamafugite magmatism and alkaline-carbonatite complexes in the Late Cretaceous Alto Paranaiba Igneous Province, Central Brazil. Internat. Geol. Rev., 1–23 https://doi.org/10.1080/00206814.2022.2127127.
Vollmer, R., Norry, M.J., 1983. Possible origin of K-rich volcanic rocks from Virunga, East Africa, by metasomatism of continental crustal material: Pb, Nd and Sr isotopic evidence. Earth Planet. Sci. Lett. 64, 374–386.
Williams, R.W., Gill, J.B., 1992. Th isotope and U-series disequilibria in some alkali basalts. Geophys. Res. Lett. 19, 139–142.
Woolley, A.R., Bergman, S.C., Edgar, A.D., Le Bas, M.J., Mitchell, R.H., Rock, N.M., Scott Smith, B.H., 1996. Classification of lamprophyres, lamproites, kimberlites, and the kalsilitic, melilitic, and leucitic rocks. Can. Mineral. 34, 175–186.
Woolley, A.R., Kempe, D.R.C., 1989. Carbonatites: nomenclature, average chemical compositions, and element distribution. In: Bell, K. (Ed.), Carbonatites: Genesis and Evolution. Unwin Hyman, London, pp. 1–14.
Woolley, A.R., Kjarsgaard, B.A., 2008. Paragenetic types of carbonatite as indicated by the diversity and relative abundances of associated silicate rocks: evidence from a global database. Can. Mineral. 46, 741–752.
Yavuz, F., 2003. Evaluating micas in petrologic and metallogenic aspect: I–definitions and structure of the computer program MICA+. Comput. Geosci. 29, 1203–1213.
Yaxley, G.M., Anenburg, M., Tappe, S., Decree, S., Guzmics, T., 2022. Carbonatites: Classification, sources, evolution and emplacement. Annu. Rev. Earth Planet. Sci. Lett. 50, 261–293.
Zartner, S., 2010. Charakterisierung und Entstehung kamafugitischer und karbonatitischer lapillituffe aus Toro-Ankole, Uganda. Unpublished Master thesis, Johannes Gutenberg-Universität Mainz.